ARTICLE

Depression compromises antiviral innate immunity via the AVP-AHI1-Tyk2 axis

Hong-Guang Zhang[1,2,9], Bin Wang[3,4,9], Yong Yang[5], Xuan Liu[6], Junjie Wang[3], Ning Xin[3], Shifeng Li[7], Ying Miao[1,2], Qiuyu Wu[1,2], Tingting Guo[1,2], Yukang Yuan[1,2], Yibo Zuo[1,2], Xiangjie Chen[1,2], Tengfei Ren[1,2], Chunsheng Dong[1,2], Jun Wang[7], Hang Ruan[1], Miao Sun[4], Xingshun Xu[3,6,8]✉ and Hui Zheng[1,2]✉

Depression is a serious public-health issue. Recent reports have suggested higher susceptibility to viral infections in depressive patients. However, how depression affects antiviral innate immune signaling remains unknown. Here, we revealed a reduction in expression of Abelson helper integration site 1 (AHI1) in the peripheral blood mononuclear cells (PBMCs) and macrophages from the patients with major depressive disorder (MDD), which leads to attenuated antiviral immune response. We found that depression-related arginine vasopressin (AVP) induces reduction of AHI1 in macrophages. Further studies demonstrated that AHI1 is a critical stabilizer of basal type-I-interferon (IFN-I) signaling. Mechanistically, AHI1 recruits OTUD1 to deubiquitinate and stabilize Tyk2, while AHI1 reduction downregulates Tyk2 and IFN-I signaling activity in macrophages from both MDD patients and depression model mice. Interestingly, we identified a clinical analgesic meptazinol that effectively stimulates AHI1 expression, thus enhancing IFN-I antiviral defense in depression model mice. Our study promotes the understanding of the signaling mechanisms of depression-mediated antiviral immune dysfunction, and reveals meptazinol as an enhancer of antiviral innate immunity in depressive patients.

Cell Research (2022) 32:897–913; https://doi.org/10.1038/s41422-022-00689-9

INTRODUCTION

Depression is one of the leading causes of years lived with disability worldwide. Patients with major depressive disorder (MDD) show great decrements in quality of life, and ~15% of MDD patients ultimately die of suicide.[1,2] Depression often induces or worsens other associated diseases.[3] To date, limited studies on depression and virus infection have only suggested their correlation. Depression is reported to be associated with the disease progression and increased complications of some viral infections such as severe acute respiratory syndrome coronavirus 2 (SARS-CoV-2) and human immunodeficiency virus (HIV).[4–6] In addition, several studies reported that MDD patients have a higher risk to infection of viruses, including herpes zoster,[7,8] suggesting that depression could increase susceptibility to viral infection. As a matter of fact, viral infection in turn promotes the occurrence and development of depression.[9,10] Therefore, viral infection is considered a severe threat to depressive patients. However, whether and how depression affects antiviral innate immune signaling remains unexplored.

Antiviral innate immunity is the first line of defense against viral infection. Upon infection, the pattern recognition receptors (PRRs) of innate immune cells can recognize the pathogen-associated molecular patterns (PAMPs) of the viruses, leading to type-I interferon (IFN-I) production.[11–13] IFN-I then binds to a type-I IFN receptor (IFNAR) that consists of two chains (IFNAR1 and IFNAR2), which are present on the cell surface of almost all types of cells. Upon binding, IFN-I induces tyrosine phosphorylation of Janus kinase (JAK1 and Tyk2). JAK1 and Tyk2 further activate STAT1 and STAT2 to form the ISGF3 complex with IRF9, which translocates into the nucleus to bind with IFN-stimulated response elements (ISRE) in the promoter of IFN-stimulated genes (ISGs), and eventually induces expression of hundreds of ISGs to promote antiviral innate immunity.[14–17] Recently, the regulation of the stability of basal IFN signaling has received great attention due to its crucial roles in controlling numerous physiological or pathological responses, whereas IFN signaling is widely disturbed by internal environmental factors (such as inflammatory cytokines and the tumor microenvironment) in the body, leading to instability and dysregulation of basal IFN signaling.[18–20] Therefore, revealing the regulation of basal IFN-I signaling stability is of great significance for understanding the immune dysfunction under different conditions. Regarding depressive patients, how depression affects the abovementioned innate immune signaling remains to be illuminated.

Here, we observed a substantial reduction in Abelson helper integration site 1 (AHI1) expression levels in not only peripheral macrophages but also lung and liver tissues from MDD patients or depressive model mice. Intriguingly, we uncovered that arginine

[1]International Institute of Infection and Immunity, Institutes of Biology and Medical Sciences, Soochow University, Suzhou, Jiangsu, China. [2]Jiangsu Key Laboratory of Infection and Immunity, Soochow University, Suzhou, Jiangsu, China. [3]Institute of Neuroscience, Soochow University, Suzhou, Jiangsu, China. [4]Institute for Fetology, the First Affiliated Hospital of Soochow University, Suzhou, Jiangsu, China. [5]Department of Psychiatry, the Affiliated Guangji Hospital of Soochow University, Suzhou, Jiangsu, China. [6]Department of Neurology, the First Affiliated Hospital of Soochow University, Suzhou, Jiangsu, China. [7]Department of Intensive Care Medicine, the First Affiliated Hospital of Soochow University, Suzhou, Jiangsu, China. [8]Jiangsu Key Laboratory of Neuropsychiatric Diseases, Soochow University, Suzhou, Jiangsu, China. [9]These authors contributed equally: Hong-Guang Zhang, Bin Wang. ✉email: xingshunxu@suda.edu.cn; huizheng@suda.edu.cn

Received: 7 February 2022 Accepted: 24 June 2022
Published online: 12 July 2022

vasopressin from depression-related hypothalamic-pituitary-adrenal (HPA) system induced AHI1 reduction in macrophages, and AHI1 reduction dramatically inhibited the expression of ISGs and attenuated host antiviral innate immunity. Further studies revealed a critical role of AHI1 in maintaining the stability of IFN-I signaling. Importantly, we identified meptazinol as an effective stimulator of AHI1 expression that strongly enhances IFN-I signaling and improves the antiviral immunity of depression model mice.

RESULTS

Depression induces AHI1 reduction that attenuates antiviral immune response

Previous studies from our group and others revealed that neuronal deficiency of AHI1, which is abundant in the hypothalamus and amygdala, is associated with depression.[21–23] We found that AHI1 was also expressed in other types of cells, including macrophages, epithelial cells and fibroblast cells. Intriguingly, *Ahi1* mRNA levels were significantly reduced in the peripheral blood mononuclear cells (PBMCs) of unmedicated MDD patients, compared with the age/sex-matched healthy control subjects (Fig. 1a). We further examined *Ahi1* mRNA expression in peripheral macrophages and T and B cells separated from PBMCs of MDD patients. The results showed that peripheral macrophages from unmedicated MDD patients exhibited the most dramatic reduction in *Ahi1* expression, although other types of cells also showed *Ahi1* reduction to some extent (Fig. 1b; Supplementary information, Fig. S1a). To confirm that depression induces *Ahi1* reduction, we used a spatial restraint stress mouse model that has been well documented to induce depression-like behaviors in mice.[21,24,25] We observed increased immobility times in the forced swim test (FST) and tail suspension test (TST) in depression model mice (DMM) (Supplementary information, Fig. S1b, c),[21] suggesting that the depression model has been established successfully. Consistent with the data from MDD patients, *Ahi1* mRNA levels in both PBMCs (Fig. 1c) and macrophages (Fig. 1d) from these depression model mice were markedly reduced, compared with those from the normal control mice. Accordingly, AHI1 protein levels in the PBMCs of depression model mice substantially decreased (Supplementary information, Fig. S1d). The lung and liver tissues of these depression model mice also showed reduced levels of AHI1 (Fig. 1e), suggesting that depression induces AHI1 reduction in multiple tissues of the body, which could probably result from the regulation by certain systemic circulation factors such as depression-related hormones.

To explore the potential significance of AHI1 reduction on immune dysfunction in MDD patients, we utilized RNA sequencing technology to analyze the differential gene expression in $Ahi1^{-/-}$ cells. Interestingly, we noticed that the vast majority of interferon-induced gene (*Ifi*) family members, e.g., *Ifit1*, *Ifit2*, *Ifit3*, *Ifi202b*, *Ifi205*, exhibited significantly lower expression in $Ahi1^{-/-}$ cells than in $Ahi1^{+/+}$ cells (Fig. 1f; Supplementary information, Fig. S1e). In addition, among the top 50 differentially expressed genes in terms of fold changes, there are many well-recognized ISGs, including *Cxcl10*, *Rsad2* (*Viperin*), *Ifi*- and *Serpin*-family members (Fig. 1g). We then confirmed the downregulation of *Ifit1* and *Rsad2*, two widely used representative ISGs, in $Ahi1^{-/-}$ cells by RT-qPCR (Supplementary information, Fig. S1f). Importantly, peripheral macrophages from the unmedicated MDD patients also displayed a significant reduction in the expression levels of the representative ISGs compared with those from healthy controls (Fig. 1h; Supplementary information, Fig. S1g). These observations suggested that AHI1 deficiency in cells could downregulate basal ISG expression.

Based on the above findings, we speculated that the antiviral ability of AHI1-deficient cells could be compromised. Thus, we first used two RNA viruses, vesicular stomatitis virus (VSV) and influenza A virus (H1N1, PR8/34), and one DNA virus-herpes simplex virus 1 (HSV-1). In line with this speculation, knockout of *Ahi1* in mouse macrophages strongly promoted infection of these viruses (Fig. 1i; Supplementary information, Fig. S2a). Similarly, downregulation of AHI1 using two specific shRNAs also facilitated VSV infection (Supplementary information, Fig. S2b). These findings implied that AHI1 reduction in unmedicated MDD patients could attenuate their antiviral defense, which could provide clues for understanding the mechanisms by which MDD patients are usually more susceptible to viral infection. Further results in depression model mice also showed that they were more susceptible to viral infection than control mice (Fig. 1j).

Given that depression results in AHI1 reduction in many types of cells and tissues, we employed AHI1-knockout ($Ahi1^{-/-}$) mice to directly study the significance of AHI1 deficiency in regulating the antiviral ability of the host. Our results showed that AHI1 deficiency in mice significantly promoted viral infection, as shown by increased virus titers in the blood of $Ahi1^{-/-}$ mice challenged with viruses for 24 h (Fig. 1k). Consistently, the spleen, liver and lung tissues of $Ahi1^{-/-}$ mice showed higher levels of viral RNAs than those of $Ahi1^{+/+}$ mice (Supplementary information, Fig. S2c). Immunofluorescence analysis of viruses (Fig. 1l) and hematoxylin-eosin (H&E) staining of virus-infected lung tissues (Supplementary information, Fig. S2d) confirmed more viruses and more severe tissue damage in $Ahi1^{-/-}$ mice. In addition, we noticed that AHI1 deficiency did not significantly affect the percentage of peripheral monocytes/macrophages in the mice (Supplementary information, Fig. S2e), suggesting that the decrease in antiviral ability of $Ahi1^{-/-}$ mice could be due to the changes of cellular antiviral immune activity but not the numbers of these cells. Taken together, these findings revealed that depression induces AHI1 reduction in multiple tissues of the body, which weakens host antiviral ability.

AHI1 deficiency attenuates IFN-I signaling and cellular antiviral innate immunity

We further explored how AHI1 deficiency affects cellular antiviral activity and host antiviral defense. AHI1 knockout in primary macrophages did not upregulate expression of both TNFα and IFNβ (Supplementary information, Fig. S3a, b), as well as virus-induced production of IFN-I (Fig. 2a). However, AHI1 deficiency significantly inhibited both basal and IFN-I-induced expression of the representative ISGs, including *Ifit1*, *Rsad2*, and *Mx1* (Fig. 2b; Supplementary information, Fig. S3c). Consistently, knockdown of AHI1 attenuated IFN-I-induced ISRE promoter activity (Supplementary information, Fig. S3d). In line with the regulation of ISG expression, AHI1 deficiency largely restricted IFN-I-induced antiviral activity in cells (Fig. 2c). Conversely, AHI1 overexpression significantly enhanced IFN-I-induced antiviral activity (Supplementary information, Fig. S3e, f). Consistently, in IFNAR1-deficient cells, AHI1 failed to significantly regulate cellular antiviral activity (Supplementary information, Fig. S3g). These findings suggested that AHI1 could regulate the strength of IFN-I-induced signaling and subsequent cellular antiviral activity.

We next collected peripheral macrophages from MDD patients, which showed significantly reduced *Ahi1* levels (Fig. 2d), to observe their responses to viral infection and IFN-I stimulation. The results showed that macrophages from these MDD patients had decreased antiviral ability, compared with those from healthy controls (Fig. 2d). Consistently, when stimulated with IFN-I, macrophages from these MDD patients showed lower expression levels of ISGs than those from healthy controls (Fig. 2e; Supplementary information, Fig. S3h).

We then turned to $Ahi1^{-/-}$ mice and depression model mice. In line with the above findings, $Ahi1^{-/-}$ mice showed much lower basal expression of ISGs in the spleen tissues (Fig. 2f), also in the lung and liver tissues (Supplementary information, Fig. S3i, j), than $Ahi1^{+/+}$ mice, suggesting that AHI1 is essential for maintaining basal IFN-I signaling. Furthermore, the responses of depression model mice to IFN-I administration were observed. Compared with normal control

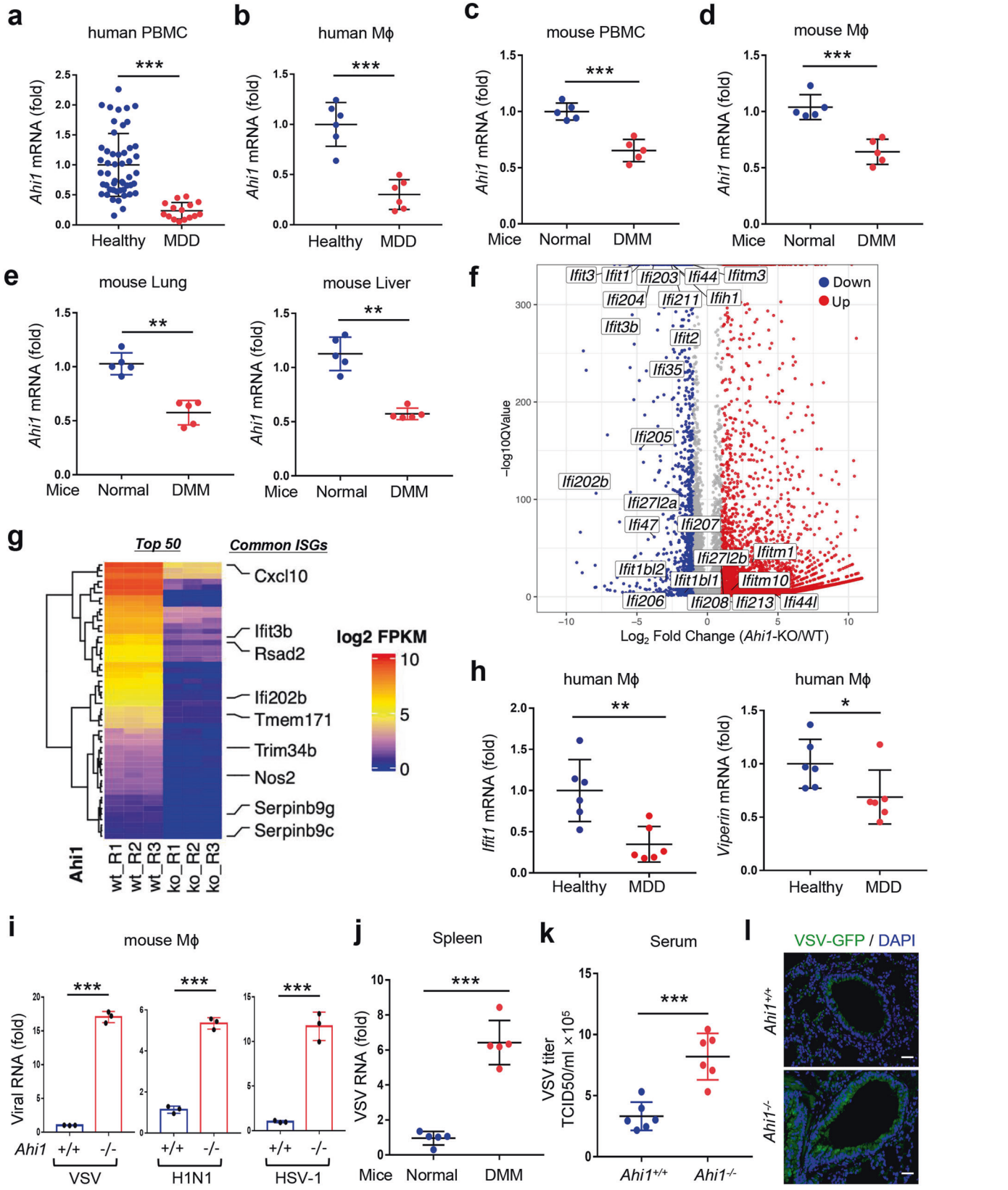

mice, depression model mice showed significantly lower expression levels of both basal ISGs and IFN-I-induced ISGs (Fig. 2g). Collectively, these findings revealed a crucial role of AHI1 in sustaining IFN-I signaling, and demonstrated that AHI1 deficiency attenuated IFN-I antiviral innate immunity.

Depression-related AHI1 deficiency lowers Tyk2 protein levels and stability

Given that AHI1 deficiency inhibits IFN-I signaling activity, we next explored the underlying mechanisms. We observed that AHI1 reduction can inhibit IFN-I-induced activation of STAT1, a central

Fig. 1 Depression induces AHI1 reduction that attenuates antiviral immune response. a RT-qPCR analysis of *Ahi1* mRNA levels in human PBMCs from healthy controls (Healthy, $n = 50$) and unmedicated MDD patients (MDD, $n = 15$). **b** RT-qPCR analysis of *Ahi1* mRNA levels in monocytes/macrophages (Mϕ) separated from PBMCs of healthy controls ($n = 6$) and unmedicated MDD patients ($n = 6$). **c**–**e** Depression model mice (DMM) were made in male ICR mice by a spatial restraint stress model for three weeks. RT-qPCR was used to analyze *Ahi1* mRNA levels in PBMCs (**c**), peritoneal macrophages (**d**), lung and liver tissues (**e**) from normal control mice (Normal, $n = 5$) or DMM ($n = 5$). **f**, **g** RNA-seq analysis of differential gene expression in $Ahi1^{+/+}$ and $Ahi1^{-/-}$ MEFs. The interferon-induced gene (IFI) family members such as *Ifit1*, *Ifit2* and *Ifi202b* (**f**) or common ISGs (**g**) were shown in volcano plots or Top 50 differential genes. **h** RT-qPCR analysis of the representative ISGs (*Ifit1* and *Viperin*) mRNA levels in human primary macrophages from PBMCs of healthy controls ($n = 6$) and unmedicated MDD patients ($n = 6$). **i** $Ahi1^{+/+}$ and $Ahi1^{-/-}$ mouse peritoneal macrophages were infected with VSV (MOI = 0.1) or H1N1/HSV-1 (MOI = 1.0) for 24 h. RT-qPCR was used to analyze viral RNA levels. **j** Normal control mice (Normal, $n = 5$) and DMM ($n = 5$) were infected with VSV (1×10^8 PFU/g of body weight, i.p.) for 24 h. RT-qPCR was used to analyze VSV viral RNA levels in the spleen tissues from the mice. **k** TCID50 assay of VSV titers in the blood from $Ahi1^{+/+}$ and $Ahi1^{-/-}$ mice ($n = 6$) infected with VSV (1×10^8 PFU/g of body weight, i.p.) for 24 h. **l** Fluorescence microscopy of VSV-GFP in the lung tissues from $Ahi1^{+/+}$ and $Ahi1^{-/-}$ mice infected with VSV-GFP as **k**. DAPI was used for the nuclear staining. Scale bars: 100 μm. ns, not significant ($P > 0.05$) and $^*P < 0.05$, $^{**}P < 0.01$ or $^{***}P < 0.001$ (two-tailed unpaired Student's *t*-test). Data are shown as means ± SD of three biological replicates (**i**). All graphs show the means ± SEM for individual persons (**a**, **b**, **h**) or mice (**c**, **d**, **e**, **j**, **k**).

signaling protein of IFN-I signaling, in both macrophages (Fig. 3a) and lung A549 cells (Supplementary information, Fig. S4a). Further analysis on the signaling molecules in IFN-I signaling upstream of STAT1 revealed that AHI1 deficiency did not affect the levels of either IFNAR1 or IFNAR2 (Fig. 3b; Supplementary information, Fig. S4b–d). AHI1 knockout in primary macrophages (Fig. 3c) or AHI1 knockdown in RAW264.7 (Fig. 3d) did not substantially affect the levels of JAK1, STAT1, STAT2 or IRF9, but dramatically lowered Tyk2 protein levels. To confirm this phenomenon, we analyzed Tyk2 protein levels in other types of $Ahi1^{-/-}$ cells. We found that Tyk2 protein levels were strongly reduced in both fibroblasts (Supplementary information, Fig. S4e) and lung epithelial tissues from $Ahi1^{-/-}$ mice (Supplementary information, Fig. S4f). These findings confirmed that AHI1 critically regulates Tyk2 protein levels in cells.

Knockdown of cellular AHI1 did not significantly affect *Tyk2* mRNA levels (Fig. 3e), suggesting that AHI1 does not regulate *Tyk2* through the transcription level. We then performed a cycloheximide (CHX) pulse chase assay to analyze Tyk2 protein stability. AHI1 deficiency remarkably accelerated Tyk2 protein degradation in both macrophages (Fig. 3f) and lung epithelial A549 cells (Supplementary information, Fig. S4g), indicating that AHI1 regulates Tyk2 protein stability. Janus kinase (Tyk2/JAK1) is named from an analogy with the two-faced Roman "God of Gates and Doors", Janus, and represents the most proximal step in IFN-I signaling.[26–28] Therefore, Tyk2 and JAK1 are considered initial and pivotal components to deliver IFN-I signaling activation. However, the delicate regulation of Tyk2 protein stability in IFN-I signaling, as well as other signaling pathways related to autoimmune diseases, remains unknown. Thus, revealing the regulation of Tyk2 stability will promote our understanding of the key mechanisms controlling the stability of IFN-I signaling.

As AHI1 was reduced in depression model mice (Fig. 1c–e), we speculated that Tyk2 proteins could also decrease in these mice. In line with this speculation, the levels of Tyk2 protein in depression model mice were notably downregulated (Fig. 3g). Moreover, we collected PBMCs from unmedicated MDD patients and found that the protein levels of Tyk2 but not another IFN-I signaling protein, STAT1, in MDD patients also noticeably decreased (Fig. 3h). Consistently, the peripheral macrophages from MDD patients that had reduced *Ahi1* levels showed lower levels of Tyk2, compared with those from healthy control (Supplementary information, Fig. S4h). Taken all together, these findings suggested that AHI1 reduction in depressive mice and humans impairs Tyk2 protein stability and subsequent IFN-I signaling activity.

AHI1 recruits OTUD1 to maintain Tyk2 protein levels

Given that AHI1 regulates Tyk2 protein stability, we proposed that AHI1 could affect ubiquitination modifications of Tyk2. Neither ubiquitin E3 ligases nor deubiquitinases of Tyk2 have been reported, we thus utilized PR-619, a broad-spectrum deubiquitinase inhibitor, to analyze whether any deubiquitinase is involved in AHI1-mediated regulation of Tyk2 levels. Interestingly, we found that PR-619 treatment completely abolished Tyk2 upregulation mediated by AHI1 (Fig. 4a), suggesting that deubiquitinases play a major role of in the AHI1-mediated increase in Tyk2 protein levels. Furthermore, by mass spectrometry analysis of the potential AHI1-interacting proteins, we noticed a deubiquitinase OTUD1, which displayed many more identified peptides in the AHI1-overexpressing group than in the vector control group (Fig. 4b). Next, we confirmed the interaction between AHI1 and OTUD1, as well as Tyk2, in both primary macrophages (Fig. 4c) and A549 cells (Supplementary information, Fig. S5a).

OTUD1 as a deubiquitinase has recently been reported to regulate the levels of several proteins.[24,29–31] We found that OTUD1 overexpression increased Tyk2 protein levels in a dose-dependent manner (Supplementary information, Fig. S5b), while OTUD1 knockout in primary macrophages dramatically reduced Tyk2 protein levels (Fig. 4d). Importantly, OTUD1 knockdown inhibited the AHI1-mediated upregulation of Tyk2 levels (Fig. 4e), suggesting that OTUD1 is essential for the AHI1-mediated regulation of Tyk2 protein levels. We noticed that AHI1 did not strongly affect OTUD1 protein levels (Fig. 4f) but affected the interaction between OTUD1 and Tyk2, as shown by the abolishment of the OTUD1-Tyk2 interaction upon AHI1 knockout in primary macrophages (Fig. 4g). Consistently, the spleen tissues of depression model mice displayed lower AHI1 levels and less interaction between OTUD1 and Tyk2 than those of normal mice (Fig. 4h). However, OTUD1 deficiency did not strongly affect the AHI1-Tyk2 interaction (Supplementary information, Fig. S5c). These findings suggested that Tyk2 can interact with AHI1, which recruits OTUD1 to maintain Tyk2 protein levels. Collectively, our results demonstrated a critical role of OTUD1 in maintaining AHI1-mediated regulation of Tyk2 protein levels.

OTUD1 regulates the K48-linked polyubiquitination of Tyk2 dependently on AHI1

To reveal the role of the deubiquitinase OTUD1 in AHI1-mediated regulation of Tyk2, we further determined the effects of OTUD1 on Tyk2 ubiquitination. We found that the deubiquitinase-inactive mutant of OTUD1 (OTUD1-C_{320}A-H_{431}Q, CH)[24] lost the ability to upregulate Tyk2 protein levels (Fig. 5a), suggesting that OTUD1 could regulate Tyk2 ubiquitination. In line with this, OTUD1 deficiency in both primary macrophages (Fig. 5b) and MEFs (Supplementary information, Fig. S5d), as well as A549 cells (Supplementary information, Fig. S5e), markedly improved Tyk2 ubiquitination levels, whereas OTUD1 overexpression inhibited Tyk2 ubiquitination (Fig. 5c; Supplementary information, Fig. S5f). Importantly, AHI1 deficiency inhibited OTUD1-mediated both downregulation of Tyk2 ubiquitination (Fig. 5c) and upregulation of Tyk2 protein levels (Supplementary information, Fig. S5g), suggesting that OTUD1 regulates Tyk2 ubiquitination and protein levels dependently on AHI1.

OTUD1 has been reported to be able to regulate both K48-linked and K63-linked ubiquitination of protein substrates.[24] We then

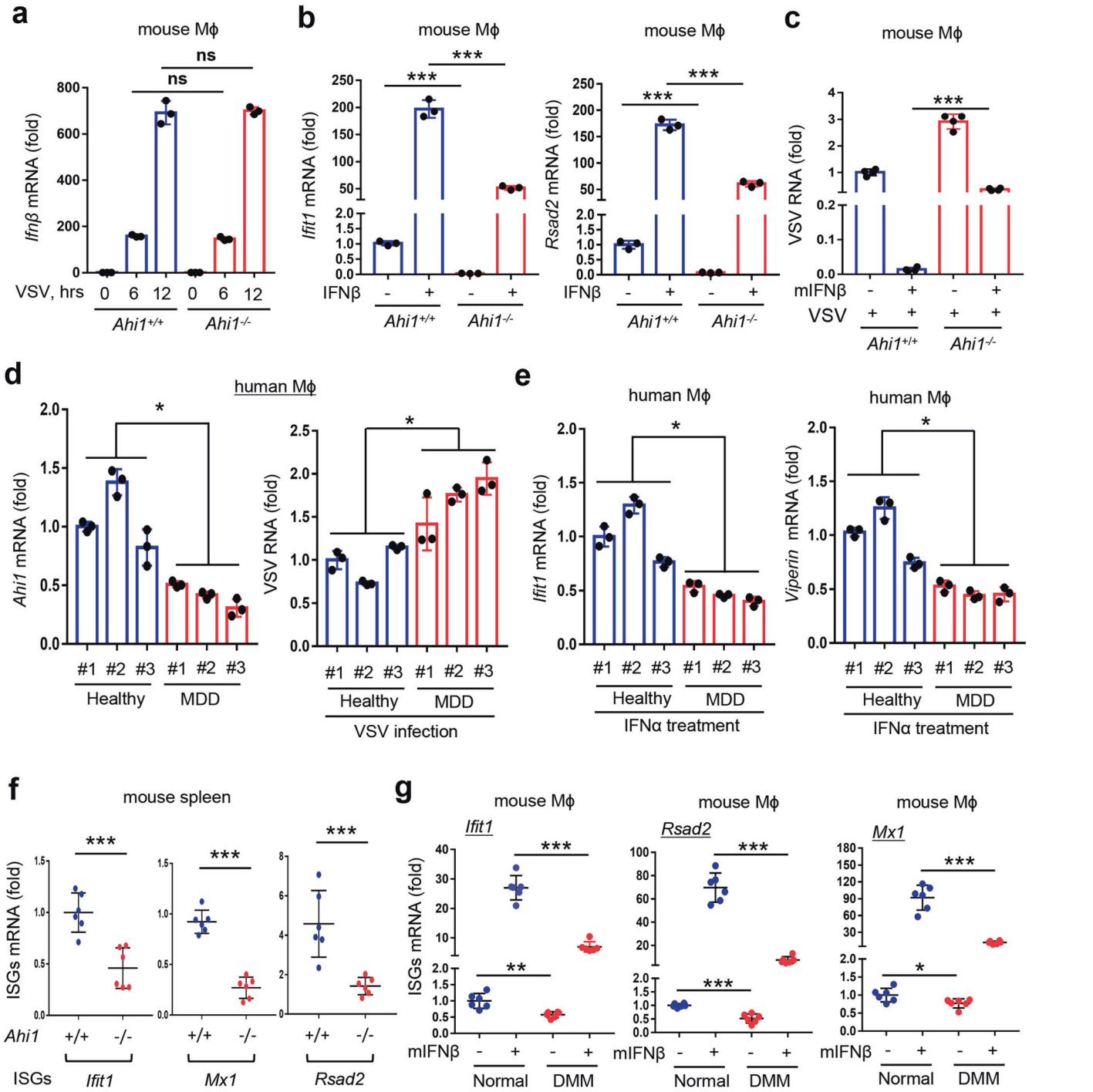

Fig. 2 AHI1 deficiency lowers IFN-I signaling and cellular antiviral innate immunity. a RT-qPCR analysis of *Ifnβ* mRNA levels in *Ahi1*$^{+/+}$ and *Ahi1*$^{-/-}$ mouse peritoneal macrophages infected with VSV (MOI = 0.1) for 0, 6, 12 h. **b** RT-qPCR analysis of the representative ISGs (*Ifit1* and *Rsad2*) mRNA levels in *Ahi1*$^{+/+}$ and *Ahi1*$^{-/-}$ mouse peritoneal macrophages stimulated with mouse IFNβ (mIFNβ, 1000 IU/mL) for 8 h. **c** Mouse peritoneal macrophages from *Ahi1*$^{+/+}$ and *Ahi1*$^{-/-}$ mice were stimulated with mIFNβ (40 IU/mL) for 20 h and then were infected with VSV (MOI = 0.1) for 24 h. RT-qPCR was used to analyze VSV RNA levels. **d** RT-qPCR was used to analyze *Ahi1* mRNA levels in human primary macrophages from PBMCs of healthy donors (#1, #2, and #3) and unmedicated MDD donors (#1, #2, and #3) (left). Human primary macrophages from the above donors were infected with VSV (MOI = 0.1) for 24 h. RT-qPCR was used to analyze viral RNA levels (right). **e** Human macrophages from the above donors (**d**) were stimulated with IFNα (1000 IU/mL) for 8 h. RT-qPCR was used to analyze the representative ISGs (*Ifit1* and *Viperin*) mRNA levels. **f** RT-qPCR analysis of the representative ISGs mRNA in the spleen tissues from *Ahi1*$^{+/+}$ and *Ahi1*$^{-/-}$ mice. **g** RT-qPCR analysis of the representative ISGs mRNA in peritoneal macrophages from normal control mice (Normal) and depression model mice administrated with mIFNβ (1500 IU/g, i.p.) for 8 h. ns, not significant ($P > 0.05$) and $^{*}P < 0.05$, $^{**}P < 0.01$, $^{***}P < 0.001$ (two-tailed unpaired Student's *t*-test). Data are shown as means ± SD of three or four biological replicates (**a**, **b**, **c**). All graphs show the means ± SEM for individual persons (**d**, **e**) or six individual mice (**f**, **g**).

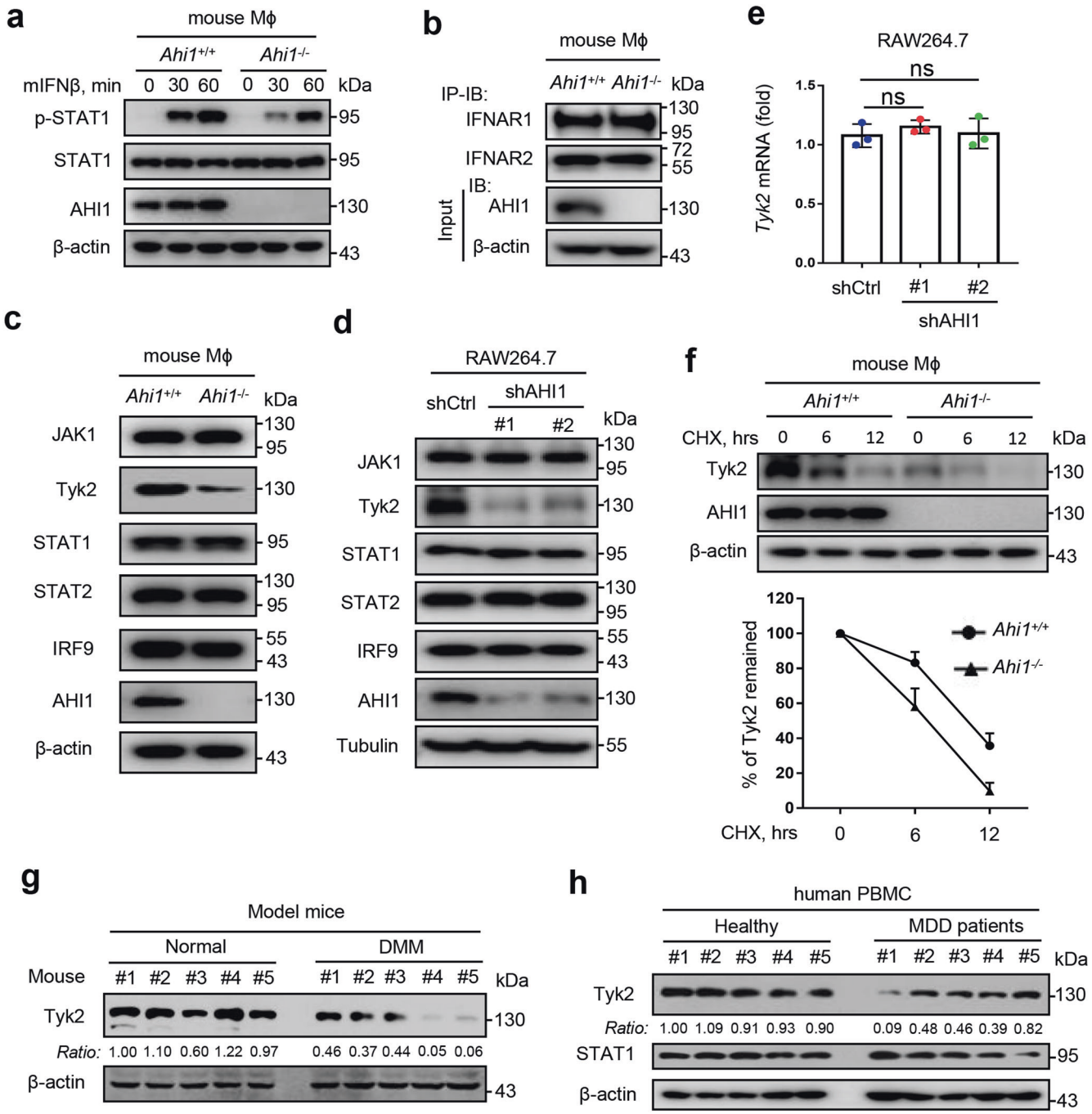

Fig. 3 Depression-related AHI1 deficiency lowers Tyk2 protein levels and stability. a Western blot analysis of Tyr701 phosphorylation of STAT1 (p-STAT1) in *Ahi1*$^{+/+}$ and *Ahi1*$^{-/-}$ mouse peritoneal macrophages treated with mIFNβ (1000 IU/mL). **b** Western blot analysis of IFNAR1 and IFNAR2 protein levels in *Ahi1*$^{+/+}$ and *Ahi1*$^{-/-}$ mouse peritoneal macrophages. **c** Western blot analysis of the JAK-STAT signaling proteins (JAK1, Tyk2, STAT1, STAT2 and IRF9) in *Ahi1*$^{+/+}$ and *Ahi1*$^{-/-}$ mouse peritoneal macrophages. **d** Western blot analysis of the JAK-STAT signaling proteins (JAK1, Tyk2, STAT1, STAT2 and IRF9) in RAW264.7 cells transfected with either control shRNAs (shCtrl) or two specific shRNAs against AHI1 (shAHI1: #1, #2). **e** RT-qPCR analysis of *Tyk2* mRNA levels in RAW264.7 cells transfected with either shCtrl or two specific shAHI1 (#1, #2). **f** Western blot analysis of Tyk2 protein levels in *Ahi1*$^{+/+}$ and *Ahi1*$^{-/-}$ mouse peritoneal macrophages treated with cycloheximide (CHX, 50 μg/mL) for durations. **g** Western blot analysis of Tyk2 protein levels in the spleen tissues from normal control mice (Normal, $n = 5$) or depression model mice ($n = 5$). The ratio values indicate Tyk2/β-actin densitometric ratios analyzed by the ImageJ program. **h** Western blot analysis of Tyk2 and STAT1 protein levels in human PBMCs from healthy controls (Healthy, $n = 5$) and MDD patients ($n = 5$). ns, not significant ($P > 0.05$) (two-tailed unpaired Student's *t*-test). Data are shown as means ± SD of three biological replicates (**e**, **f**), or are representative of three independent experiments (**a**–**d**, **f**–**h**).

analyzed the type(s) of ubiquitination of Tyk2 regulated by OTUD1, and found that OTUD1 overexpression dramatically reduced K48-linked ubiquitination of Tyk2 (Fig. 5d), while OTUD1 knockout increased K48-linked polyubiquitination of Tyk2 (Fig. 5e), which was consistent with the upregulation of Tyk2 K48-linked polyubiquitination mediated by AHI1 knockout (Fig. 5f). Taken all together, these findings proved that OTUD1 regulates Tyk2 K48-linked polyubiquitination and protein levels in an AHI1-dependent manner.

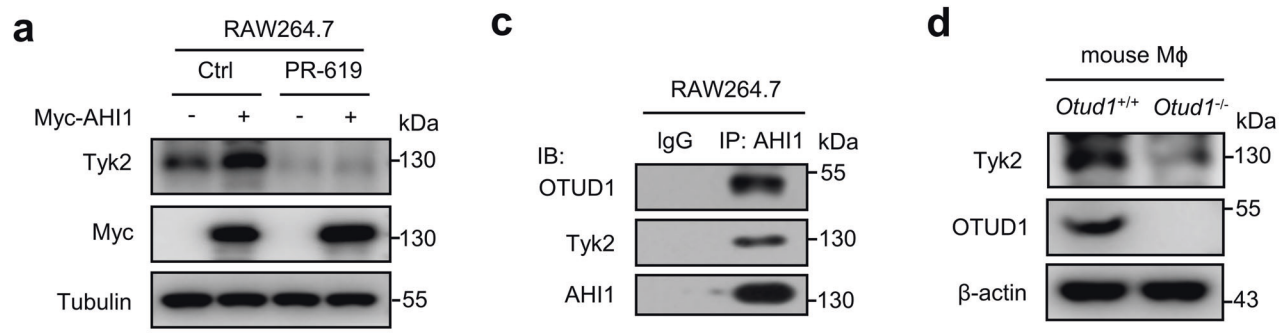

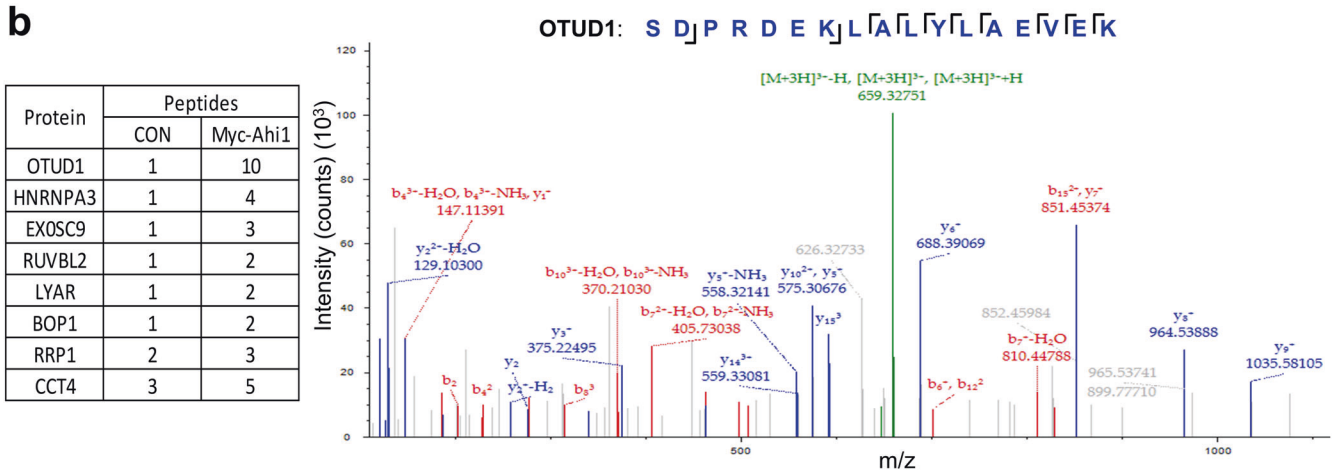

Protein	Peptides	
	CON	Myc-Ahi1
OTUD1	1	10
HNRNPA3	1	4
EX0SC9	1	3
RUVBL2	1	2
LYAR	1	2
BOP1	1	2
RRP1	2	3
CCT4	3	5

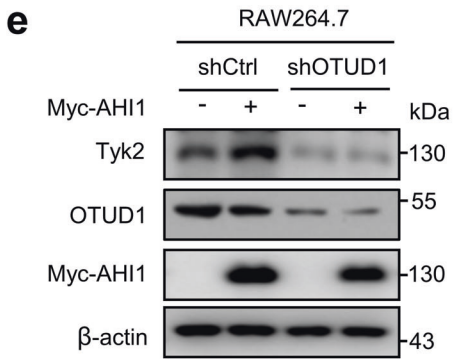

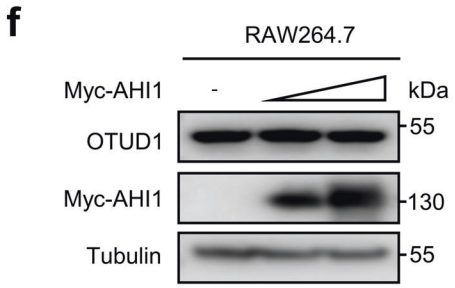

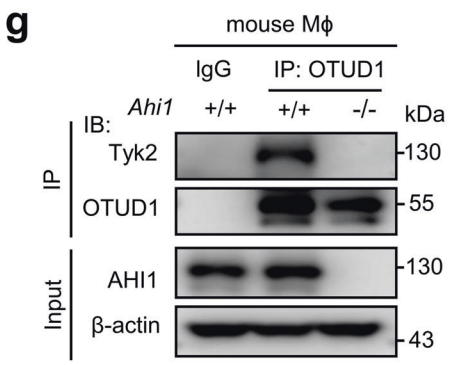

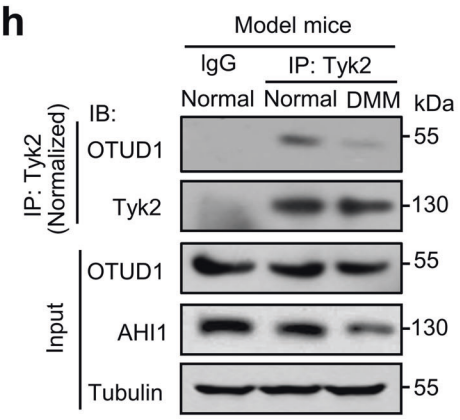

Depression-elevated arginine vasopressin induces AHI1 reduction and inhibits IFN-I antiviral signaling

Alterations in hormones and endocrine function have been considered to be essential to development of the pathophysiology of MDD. Based on the commonly recognized HPA system that plays key roles in depression, we first analyzed the effects of several hormones, including adrenocorticotropic hormone (ACTH), AVP and glucocorticoids, which can be secreted into peripheral circulation from the HPA system. The results showed that AVP, but neither ACTH nor the glucocorticoid dexamethasone (Dex), significantly

Fig. 4 AHI1 can recruit OTUD1 to maintain Tyk2 protein levels. a Western blot analysis of Tyk2 protein levels in RAW264.7 cells transfected with Myc-AHI1 and then treated with a pan-deubiquitinase inhibitor PR-619 (50 μM) for 2 h. **b** Mass spectrometry analysis of the potential Myc-AHI1-binding proteins in A549 cells. The number of the identified peptides from the interacting proteins including OTUD1 were shown as indicated (left). The secondary peptide mass spectrum of OTUD1 protein was shown (right). **c** Immunoprecipitation analysis of the binding of endogenous AHI1 with OTUD1, as well as Tyk2 in RAW264.7 cells. **d** Western blot analysis of Tyk2 protein levels in peritoneal macrophages from *Otud1*$^{+/+}$ and *Otud1*$^{-/-}$ mice. **e** Western blot analysis of Tyk2 protein levels in RAW264.7 cells cotransfected with either shCtrl or shOTUD1, together with Myc-AHI1 as indicated. **f** Western blot analysis of endogenous OTUD1 protein levels in RAW264.7 cells transfected with increasing amounts of Myc-AHI1. **g** Immunoprecipitation analysis of the interaction between endogenous OTUD1 and Tyk2 in *Ahi1*$^{+/+}$ and *Ahi1*$^{-/-}$ mouse peritoneal macrophages. **h** Immunoprecipitation analysis of the interaction between endogenous Tyk2 and OTUD1 in the spleen tissues from normal control mice (Normal) or depression model mice. All data are representative of three independent experiments.

downregulated *Ahi1* mRNA levels in macrophages (Fig. 6a). Furthermore, AVP, but not ACTH or Dex, dramatically lowered protein levels of both AHI1 and Tyk2 in both primary macrophages and RAW264.7 in a dose-dependent manner (Fig. 6b; Supplementary information, Fig. S6a–c). Moreover, the effect of AVP on AHI1 was dependent on the AVP receptor, since the antagonist for AVP receptor types 1a and 2, conivaptan, abolished AVP-mediated AHI1 reduction (Fig. 6c). In fact, AVP has been reported to be upregulated in depression patients.[32] Our data showed that MDD patients did have higher serum AVP levels than the healthy controls (Fig. 6d). In depression model mice, serum AVP levels also increased compared with those in the normal controls (Fig. 6e). Importantly, we found that AVP-induced downregulation of Tyk2 protein levels in primary macrophages was dependent on AHI1 (Fig. 6f).

Combining the above results, we speculated that elevated levels of AVP could contribute to the decrease in AHI1 and Tyk2, which could inhibit IFN-I signaling and antiviral activity. Consistent with this speculation, AVP inhibited the expression of not only basal ISGs but also exogenous IFN-I-induced ISGs (Fig. 6g). AVP treatment promoted viral infection (Fig. 6h, i), and inhibited IFN-I-induced antiviral activity (Fig. 6j). In addition, we demonstrated that AVP did not significantly affect the replication of the virus itself in primary macrophages (Supplementary information, Fig. S6d) or the ability of the virus to enter cells (Supplementary information, Fig. S6e). Next, we analyzed whether AVP regulated *Ahi1* mRNA reduction in vivo. Administration with AVP (50 ng/kg) for 2 days resulted in reduced *Ahi1* mRNA expression in PBMCs of mice (Fig. 6k). Consistently, Tyk2 protein levels in mouse spleen tissues also decreased upon AVP treatment (Fig. 6l). Importantly, we observed that AVP administration in mice significantly lowered expression of in vivo ISGs, including *Ifit1*, *Rsad2* and *Mx1* (Fig. 6m). Collectively, these findings suggested that depression-elevated AVP contributes to AHI1 and Tyk2 reduction, which in turn inhibits IFN-I signaling activity and eventually attenuates antiviral innate immunity of the host.

Meptazinol promotes AHI1 expression and enhances cellular IFN-I antiviral activity

Our above findings revealed that depression-mediated downregulation of AHI1 results in attenuated antiviral innate immunity. Thus, we further explored potential strategies to improve AHI1 levels for enhancement of IFN-I antiviral activity. By screening some available clinical drugs, we noticed that a potent analgesic, meptazinol, significantly promoted *Ahi1* mRNA expression in primary macrophages (Fig. 7a), RAW264.7 (Supplementary information, Fig. S7a, b) and A549 cells (Supplementary information, Fig. S7c, d) in a dose-dependent and time-dependent manner. Consistently, protein levels of both AHI1 and Tyk2 were upregulated by meptazinol (Fig. 7b). AHI1 knockout abolished meptazinol-induced upregulation of Tyk2 protein levels (Fig. 7c), suggesting that meptazinol regulates Tyk2 levels through AHI1. Furthermore, meptazinol remarkably upregulated AHI1 mRNA and protein levels, as well as Tyk2 protein levels in primary macrophages (Fig. 7d, e), lung epithelial and fibroblast cells (Supplementary information, Fig. S7e) from depression model mice. Moreover, the levels of both AHI1 (Fig. 7f) and Tyk2 (Fig. 7g) in primary macrophages from MDD patients were upregulated by meptazinol. However, we noticed that meptazinol did not significantly affect mRNA levels of Tyk2 (Supplementary information, Fig. S7f, g) or OTUD1 (Supplementary information, Fig. S7h, i), as well as the μ-opioid receptor for meptazinol (Supplementary information, Fig. S7j) in primary macrophages from either depression model mice or MDD patients. These findings demonstrated that meptazinol efficiency promotes AHI1 expression, which leads to upregulation of Tyk2 protein.

We further determined the effects of meptazinol on cellular IFN-I signaling and IFN-I-induced antiviral activity, uncovering that meptazinol treatment strongly promoted IFN-I-induced expression of the representative ISGs, including *Ifit1*, *Rsad2* and *Isg15*, in primary macrophages (Fig. 7h). We then analyzed the meptazinol-mediated regulation of IFN-I antiviral activity. Consistent with the upregulation of ISGs, meptazinol treatment restricted viral infection in a dose-dependent manner (Supplementary information, Fig. S7k). Importantly, IFN-I-induced antiviral activity against both VSV (Fig. 7i) and H1N1 (Fig. 7j) can be improved by meptazinol, whereas knockout of *Ahi1* gene blocked meptazinol-induced improvement of IFN-I antiviral activity (Fig. 7i, j). We also noticed that in *Ifnar1*$^{-/-}$ cells, meptazinol lost the ability to enhance IFN-I antiviral activity (Supplementary information, Fig. S7l). In addition, meptazinol did not significantly affect the replication of the virus itself (Supplementary information, Fig. S7m) or the ability of the virus to enter cells (Supplementary information, Fig. S7n). Taken all together, these findings suggested that meptazinol upregulates Tyk2 protein levels by promoting AHI1 expression, which improves cellular IFN-I signaling and IFN-I antiviral activity.

Meptazinol enhances the in vivo antiviral immunity of depression model mice

We next observed the in vivo effects of meptazinol on AHI1 and Tyk2 levels, as well as host antiviral immunity, in depression model mice. Meptazinol did not result in noticeable cytotoxicity in primary macrophages from either controls or depression model mice (Supplementary information, Fig. S8a). Then, depression model mice were injected with or without meptazinol (10 mg/kg) for two days. We found that depression model mice displayed lower *Ahi1* mRNA expression than normal controls, while meptazinol administration significantly improved the levels of *Ahi1* mRNA in the spleen (Fig. 8a), lung and liver tissues of depression model mice (Supplementary information, Fig. S8b, c). Consistently, meptazinol administration upregulated the protein levels of both AHI1 and Tyk2 (Fig. 8b) in depression model mice. However, meptazinol did not upregulate serum AVP levels in depression model mice (Supplementary information, Fig. S8d). We further found that meptazinol administration in depression model mice promoted the expression of basal ISGs (Supplementary information, Fig. S8e). Moreover, when depression model mice were challenged by viruses, meptazinol administration significantly upregulated the expression levels of ISGs in both the spleen (Fig. 8c) and lung (Fig. 8d) tissues of depression model mice, and suppressed viral levels (Fig. 8e). The significant reduction in virus titers in the blood from depression model mice confirmed that host antiviral immunity was enhanced by meptazinol treatment (Fig. 8f, g). Together, these findings demonstrated that meptazinol administration in mice upregulates

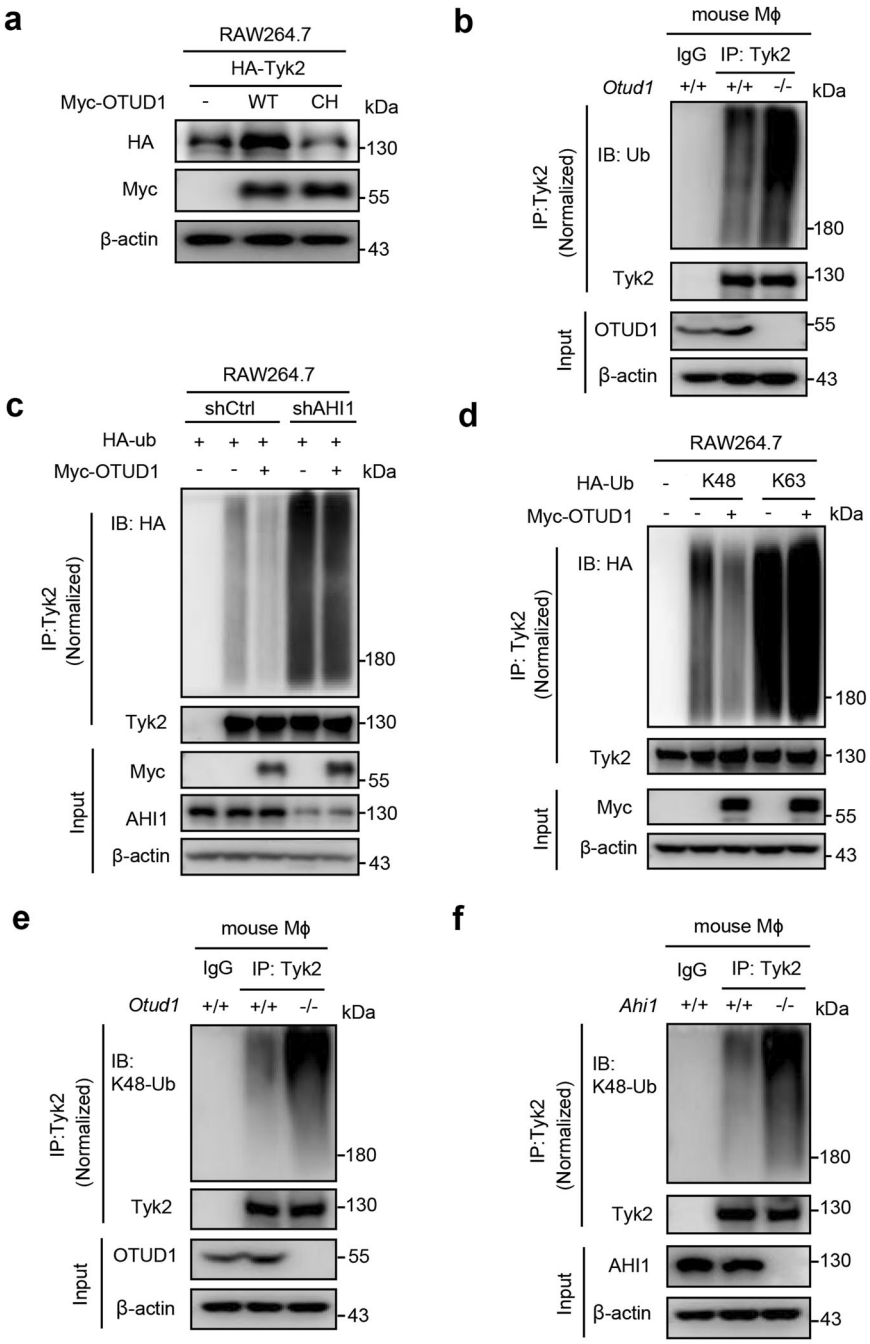

Fig. 5 OTUD1 inhibits K48-linked polyubiquitination of Tyk2 dependently on AHI1. a Western blot analysis of HA-Tyk2 levels in RAW264.7 cells cotransfected with HA-Tyk2 and Flag-OTUD1 (WT, wild-type; CH, the C320A-H431Q mutant). **b** Immunoprecipitation analysis of polyubiquitination of endogenous Tyk2 in *Otud1*$^{+/+}$ and *Otud1*$^{-/-}$ mouse peritoneal macrophages. **c** Immunoprecipitation analysis of Tyk2 polyubiquitination in RAW264.7 cells transfected with either shCtrl or shAHI1, together with or without Myc-OTUD1. **d** Immunoprecipitation analysis of the polyubiquitination types of Tyk2 in RAW264.7 cells cotransfected with Myc-OTUD1 and HA-Ub-K48 (K48-only ubiquitin) or HA-Ub-K63 (K63-only ubiquitin) as indicated. **e** Immunoprecipitation analysis of K48-linked polyubiquitination of endogenous Tyk2 in *Otud1*$^{+/+}$ and *Otud1*$^{-/-}$ mouse peritoneal macrophages using a specific anti-K48-Ub antibody. **f** Immunoprecipitation analysis of K48-linked polyubiquitination of endogenous Tyk2 in *Ahi1*$^{+/+}$ and *Ahi1*$^{-/-}$ mouse peritoneal macrophages using a specific anti-K48-Ub antibody. All data are representative of three independent experiments.

AHI1 and Tyk2 levels, and largely rescues depression-mediated inhibition of host antiviral immunity.

DISCUSSION

Depression impairs multiple systems of the body, including immune system. In the last two decades, studies have focused on how immune inflammatory responses influence the central nervous system and contribute to the pathophysiology of MDD.[8,33–36] Although the effects of depression on the immune composition and some immune functions have recently been under preliminary observation, the conclusions from these studies are often inconsistent and even controversial.[37–40] In this work, we focused on antiviral innate immune signaling, and demonstrated that

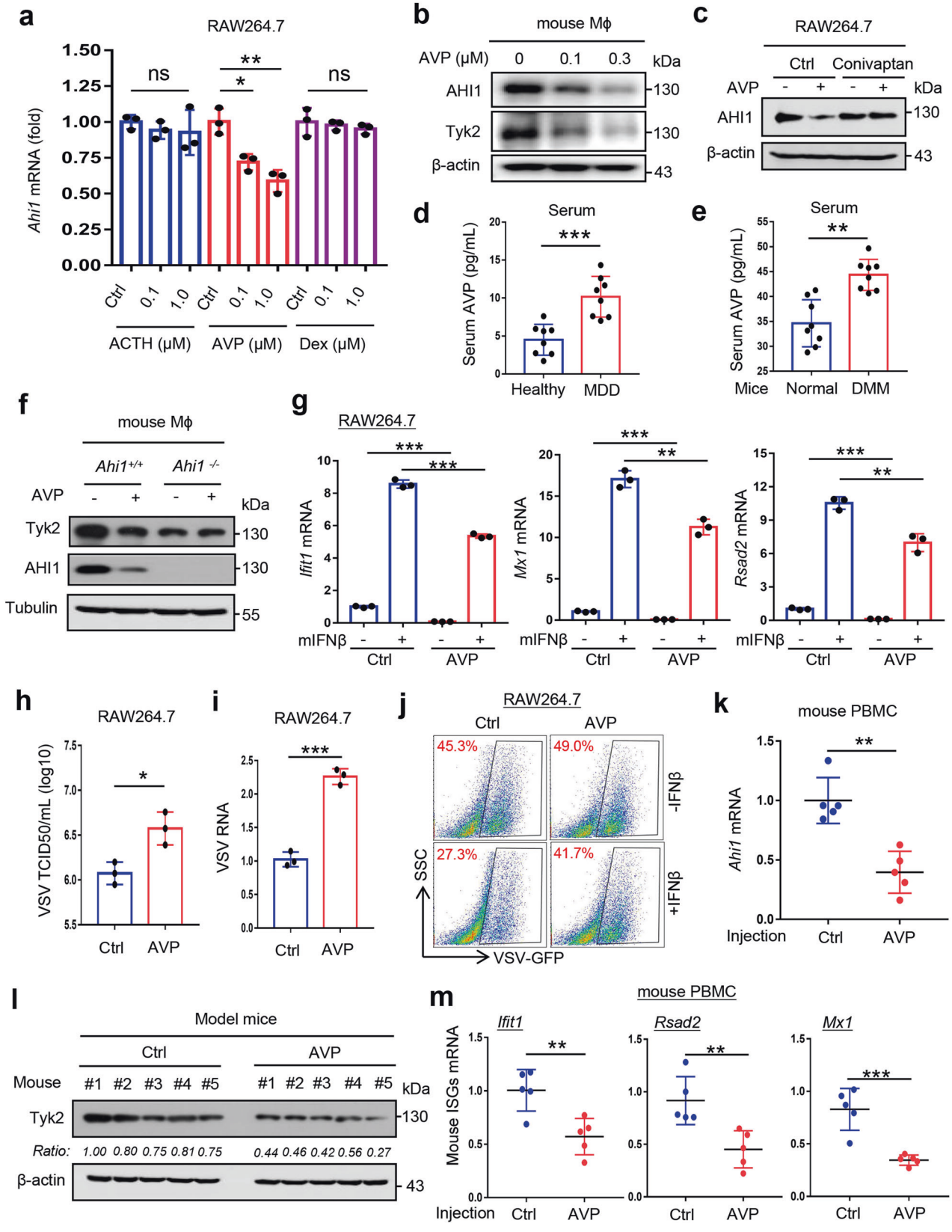

depression compromises IFN-I antiviral innate immunity through AVP-mediated disruption of the AHI1-Tyk2 axis in unmedicated MDD patients. In addition, this study revealed AHI1 as an essential stabilizer of basal IFN-I signaling in cells, which utilizes the deubiquitinase OTUD1 to protect the "God of Gates and Doors" of IFN-I signaling, Tyk2, from ubiquitination-mediated destruction.

Depression could result in specific immune responses that are different from anxiety or simple stress. Although recent studies have

Fig. 6 Depression-elevated AVP induces AHI1 reduction and inhibits IFN-I antiviral signaling. a RT-qPCR analysis of *Ahi1* mRNA levels in RAW264.7 treated with corticotropin (ACTH), or arginine vasopressin (AVP), or dexamethasone (Dex) for 24 h. **b** Western blot analysis of AHI1 and Tyk2 protein levels in mouse peritoneal primary macrophages treated with AVP (0, 0.1 and 0.3 μM) for 24 h. **c** Western blot analysis of AHI1 protein levels in RAW264.7 pretreated with DMSO (Ctrl) or an AVP-receptor inhibitor Conivaptan (10 μM) for 12 h, and then treated with AVP (0.3 μM) for 24 h. **d** The concentrations of serum AVP from healthy donors ($n = 8$) and unmedicated MDD donors ($n = 8$) were measured by an AVP ELISA kit. **e** Depression model mice were made in male ICR mice by a spatial restraint stress model for three weeks. Serum AVP concentrations from normal control mice (Normal, $n = 8$) or DMM ($n = 8$) were measured by an AVP ELISA kit. **f** Mouse peritoneal macrophages from *Ahi1*$^{+/+}$ and *Ahi1*$^{-/-}$ mice were treated with AVP (0.3 μM) for 24 h. Western blot assay was used to analyze Tyk2 and AHI1 protein levels. **g** RT-qPCR analysis of the representative ISGs (*Ifit1, Mx1* and *Rsad2*) mRNA levels in RAW264.7 treated with AVP (0.3 μM, 24 h) and then stimulated with mIFNβ (1000 IU/mL) for 8 h. **h, i** $TCID_{50}$ assay of VSV titers in the culture supernatants of RAW264.7 (**h**) or RT-qPCR analysis of VSV viral RNA in RAW264.7 (**i**) treated with AVP (0.3 μM, 24 h) and then infected with VSV (MOI = 0.1) for 24 h. **j** FACS analysis of the VSV-GFP levels in RAW264.7 treated with AVP (0.3 μM, 24 h) and then treated with mIFNβ (40 IU/mL) for 20 h, followed by infection with VSV-GFP (MOI = 0.1) for 24 h. **k** RT-qPCR analysis of *Ahi1* mRNA levels in PBMCs of mice administrated with physiological saline (Ctrl) or AVP (50 ng/kg; i.p.; once a day) for 48 h. **l** Western blot analysis of AHI1 protein levels in the spleen tissues of mice treated as **k**. **m** RT-qPCR analysis of the representative ISGs (*Ifit1, Mx1* and *Rsad2*) mRNA levels in mouse PBMCs from **k**. ns, not significant ($P > 0.05$) and $^{*}P < 0.05$, $^{**}P < 0.01$, $^{***}P < 0.001$ (two-tailed unpaired Student's *t*-test). Data are shown as means ± SD of three biological replicates (**a**, **g**–**i**), or are representative of three independent experiments (**b**, **c**, **f**, **j**, **l**). All graphs show the means ± SEM for individual persons (**d**) or individual mice (**e**, **k**, **m**).

reported the effects of depression on the numbers and activity of immune cells, most of these observations are incompatible and therefore are not enough to provide reliable clues for understanding how depression attenuates antiviral innate immunity. According to some studies, the numbers of monocytes, $CD4^+$ T and $CD8^+$ T cells in the peripheral blood of MDD patients differ from those in healthy people.[37–39] However, a study with a large sample size showed no difference in the number of peripheral blood lymphocytes or T-lymphocyte subsets and even natural killer cell (NK) activity between depressive patients and normal controls.[41] In addition, a study reported that MDD patients have increased Treg cells,[37] while another study showed that Treg cells are defective in MDD patients.[38] Moreover, no significant differences in the absolute number of circulating granulocytes, monocytes and lymphocytes, frequencies of major T cell subsets ($CD4^+$ or $CD8^+$) between MDD patients and healthy people were observed in another work.[40] These inconsistent findings suggested the possibility that MDD patients could have slight changes in the numbers and percentages of immune cells due to complex individual differences, different stages of diseases, and even whether or not the patients are receiving medical treatment, whereas the activity of certain types of immune cells could contribute in a major way to the immune dysfunction. In this study, we selected unmedicated MDD patients, and found for the first time that the peripheral macrophages of depressive patients have significantly attenuated antiviral immune activity. Importantly, our study revealed an AVP-AHI1-Tyk2 axis, as an explicit signaling mechanism, which addresses depression-mediated inhibition of antiviral immune function of peripheral macrophages and epithelial tissues.

AHI1 is associated with some neuropsychiatric and brain developmental disorders such as autism, depression and schizophrenia.[1,22,42] It has been reported that *Ahi1* conditional knockout leads to typical depressive behaviors in mice.[21,43,44] Recent studies revealed that AHI1 deficiency promotes endocytic TrkB degradation and reduces TrkB signaling in neuronal cells.[21] In addition, AHI1 deficiency also destabilizes glucocorticoid receptors (GRs) to regulate depression-related gene expression in brains.[25] These studies provide clues on understanding the correlation between AHI1-deficiency and depression. Here, we demonstrated that AHI1 is an essential stabilizer of Tyk2 protein levels, and sustains basal IFN-I signaling and host antiviral immunity. However, it is possible that AHI1 could target not only IFN-I signaling but also other signaling molecules to partially regulate antiviral immune response. In fact, AHI1-mediated regulation of GR was only reported in hippocampus cells. AHI1 does not necessarily regulate GR levels in all types of cells used in this study. In addition, GR signaling has been reported to inhibit IFN-I signaling in macrophages.[45] If AHI1 interacts and regulates GR in macrophages, AHI1 deficiency-mediated downregulation of GR should enhance IFN-I antiviral signaling, which is contrary to our findings showing that AHI1 deficiency actually inhibits IFN-I signaling. Thus, the assumed AHI1-GR regulation should not largely affect AHI1-mediated effect on IFN-I antiviral immunity in macrophages. In addition, TrkB protein is specifically highly expressed in the central nervous system, and brain-derived neurotrophic factor (BDNF) is the primary ligand and activator for TrkB,[46] making TrkB unlikely to be involved in AHI1-IFN-mediated antiviral immunity in the cells used in this study, including primary macrophage, epithelial cells and fibroblasts. We also demonstrated that AHI1 does not significantly affect cellular antiviral ability in *Ifnar1*$^{-/-}$ cells that lose the response to IFN-I, suggesting the importance of AHI1-IFN signaling in cellular innate antiviral immunity.

In addition, we revealed that depression-elevated AVP largely results in *Ahi1* mRNA reduction. These findings suggested that AVP from the HPA system leads to on the one hand neuronal AHI1 reduction in brain, which promotes occurrence of depression, and on the other hand AHI1 reduction in both peripheral macrophages and epithelial tissue cells, which attenuated host antiviral innate immunity. Interestingly, it was reported that the levels of AHI1 protein but not *AHI1* mRNA in the hippocampus of depressive mice are reduced, which results from glucocorticoid-induced GR signaling.[25] However, our results showed that the glucocorticoid did not reduce the levels of *AHI1* mRNA or AHI1 protein in macrophages. These differences suggest that macrophages and hippocampus cells have different signaling responses in regulating AHI1 expression. It will be interesting to clarify the signaling crosstalk between different types of cells stimulated by different hormones in the future.

In summary, we found that depression-elevated AVP induces AHI1 reduction in macrophages, which further disrupts the deubiquitinase OTUD1-mediated stabilization of cellular Tyk2, thus attenuating basal IFN-I signaling and host antiviral immune defense (Fig. 8h). This study revealed a detailed mechanism of depression-mediated antiviral immunity dysfunction, promoting the understanding of high susceptibility to virus infection in depressive patients. Importantly, meptazinol was identified as a potent drug for increasing AHI1 expression, which eventually improves cellular IFN-I signaling and rescues antiviral immunity of depression model mice. Given that MDD patients are at high risk of viral infection, which further exacerbates the progression of the MDD disease, our findings could provide strategies for both relieving symptoms of MDD patients and ameliorating their life quality.

MATERIALS AND METHODS

Human samples

This study included 66 healthy donors (20–68 years old, mean = 36; 37 females and 29 males) from the First Affiliated Hospital of Soochow

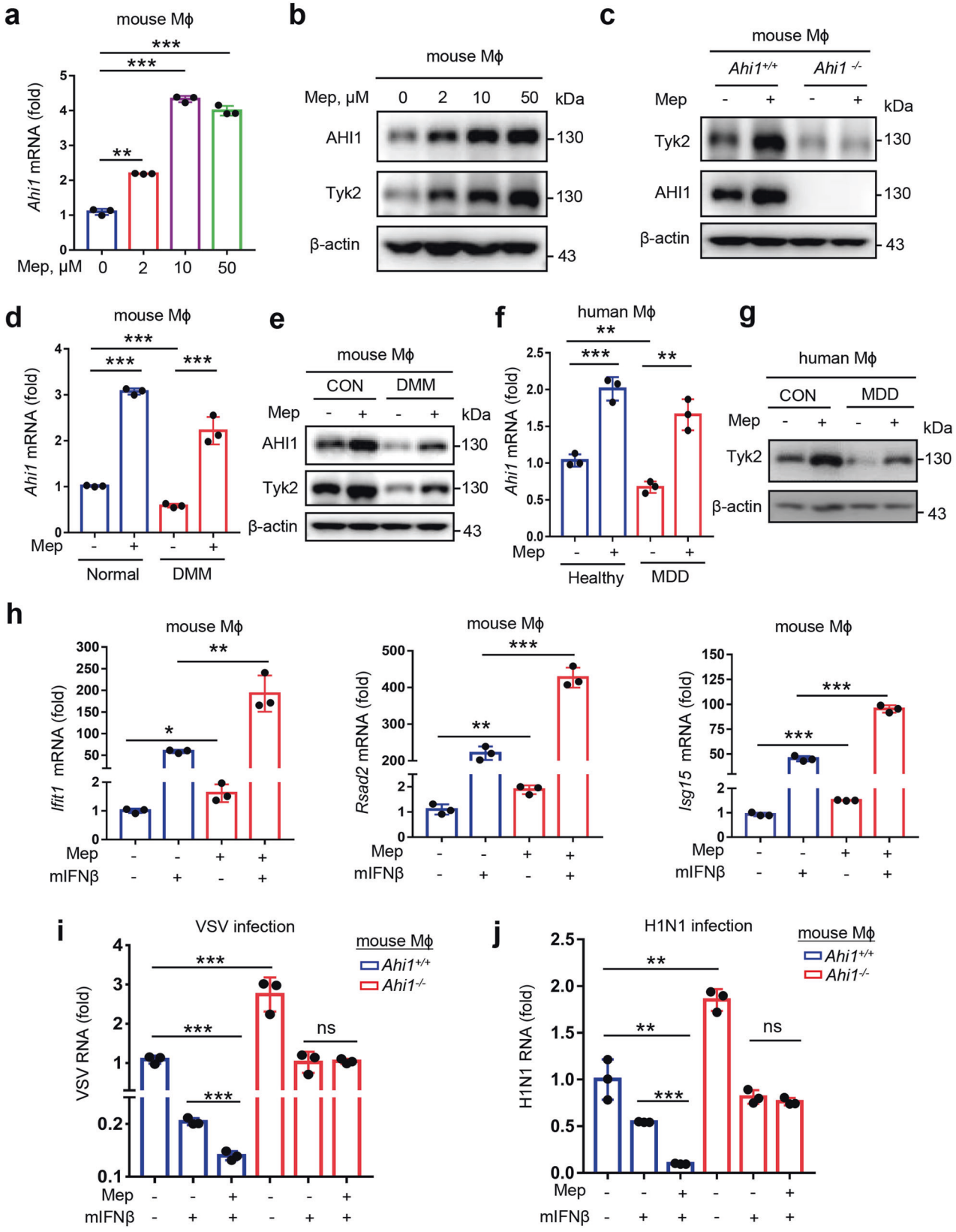

University and 31 MDD patients (16–65 years old, mean = 33; 17 females and 14 males) from either the First Affiliated Hospital of Soochow University or the Affiliated Guangji Hospital of Soochow University. Informed consent was obtained from all subjects. The study was approved by the Research Ethics Committee of the Affiliated Guangji Hospital of Soochow University (No. 2016010) and the Research Ethics Committee of the First Affiliated Hospital of Soochow University (No. 2022248). MDD patients were determined depression diagnosed by the Diagnostic and Statistical Manual of Mental Disorders, Fifth Edition (DSM-5) at the First Affiliated Hospital of Soochow University and the Affiliated Guangji

Fig. 7 Meptazinol promotes AHI1 expression to enhance cellular IFN-I antiviral activity. a RT-qPCR analysis of *Ahi1* mRNA levels in mouse peritoneal macrophages treated with meptazinol (Mep: 0, 2, 10 and 50 μM) for 24 h. **b** Western blot analysis of AHI1 and Tyk2 protein levels in mouse peritoneal macrophages treated with Mep as **a**. **c** Peritoneal macrophages from $Ahi1^{+/+}$ and $Ahi1^{-/-}$ mice were treated with Mep (10 μM) for 24 h. Western blot assay was used to analyze Tyk2 and AHI1 protein levels. **d** Peritoneal macrophages from normal and depression mode mice were treated with Mep (10 μM) for 24 h. RT-qPCR was used to analyze *Ahi1* mRNA levels. **e** Peritoneal macrophages from normal and depression model mice were treated with Mep (10 μM) for 24 h. Western blot was used to analyze AHI1 and Tyk2 protein levels. **f**, **g** Peripheral macrophages from healthy donors and unmedicated MDD donors were treated with Mep (10 μM) for 24 h. RT-qPCR was used to analyze *Ahi1* mRNA levels (**f**) and western blot assay was used to analyze Tyk2 protein levels (**g**). **h** RT-qPCR analysis of the representative ISGs (*Ifit1*, *Isg15* and *Rsad2*) mRNA levels in mouse peritoneal macrophages treated with Mep (10 μM, 24 h) and then stimulated with mIFNβ (1000 IU/mL) for 8 h. **i** RT-qPCR analysis of VSV RNA levels in $Ahi1^{+/+}$ and $Ahi1^{-/-}$ mouse peritoneal macrophages treated with Mep (10 μM, 24 h) and then stimulated with mIFNβ (40 IU/mL, 20 h), followed by infection with VSV (MOI = 0.1, 24 h) as indicated. **j** RT-qPCR analysis of H1N1 RNA levels in $Ahi1^{+/+}$ and $Ahi1^{-/-}$ mouse peritoneal macrophages treated with Mep (10 μM, 24 h) and then stimulated with mIFNβ (40 IU/mL, 20 h), followed by infection with H1N1 (MOI = 1.0, 24 h) as indicated. ns, not significant ($P > 0.05$) and $^{*}P < 0.05$, $^{**}P < 0.01$, $^{***}P < 0.001$ (two-tailed unpaired Student's *t*-test). Data are shown as means ± SD of three biological replicates (**a**, **d**, **f**, **h**–**j**), or are representative of three independent experiments (**b**, **c**, **e**, **g**).

Hospital of Soochow University. All patients were first-onset patients with depression, and none of them had taken any antidepressants. Blood samples were collected and PBMCs were isolated using a Lymphocyte Separation Medium (Da you, DAKEWE) as per manufacturer's instructions.

Mice and study approval

$Ahi1^{-/-}$ mice (C57BL/6) were from Dr. Xingshun Xu (Soochow University). $Otud1^{-/-}$ mice (C57BL/6) were generated by the Cyagen Bioscience Inc. (Guangzhou, China). Wild-type (WT) C57BL/6 and ICR mice were purchased from the Shanghai SLAC Laboratory Animals. All mice were maintained under specific-pathogen-free (SPF) conditions in the animal facility of Soochow University. 6–8-week-old mice were used in all experiments. Animal care and use protocol adhered to the National Regulations for the Administration of Affairs Concerning Experimental Animals. All animal experiments were carried out in accordance with the Laboratory Animal Management Regulations with approval (202008A520, 202108A0702) of the Scientific Investigation Board of Soochow University, Suzhou.

Establishment of depression mouse model

The male ICR mice were randomly divided into a control group (normal) and a depression model mouse group. The mice were put into the device, and the space behavior was restricted for 2–3 h in 9:00–12:00 every morning. At the same time, the normal group fasted food and water, and continued to exercise for three weeks. (1) Forced swimming test (FST): each mouse was put into a glass cylinder (20 cm high and 15 cm in diameter) with water (14 cm in depth, 23–25 °C). The swimming test videos were taken in a 6-min section. The immobility time was recorded by a well-trained person using a stopwatch. (2) Tail suspension test (TST): all mice were suspended for 6 min by sticking the tip of the tail to a rod above the desktop (35 cm). Normal mice have obvious struggle behaviors. As to the depressive mice, the immobility time without struggling was recorded.

Human primary macrophages

Human PBMCs were isolated from healthy donors and unmedicated first-onset MDD patients via Ficoll density gradient centrifugation (Lymphocyte Separation Medium). Monocytes were isolated from PBMCs using the StemSep™ Human CD14 Positive Selection Kit (14758, Stemcell). Monocytes/macrophages were cultured in RPMI 1640 medium supplemented with 10% FBS, 1% $_L$-glutamine, and 1% penicillin–streptomycin.

Mouse peritoneal macrophages and mouse primary tissue cells

Mouse primary peritoneal macrophages were harvested from mice 4 days after injection of thioglycolate (BD) and were cultured in Dulbecco's modified Eagle's medium (DMEM) with 10% FBS. Mouse primary splenocytes were isolated from spleen tissues of $Ahi1^{+/+}$ and $Ahi1^{-/-}$ mice (C57BL/6), normal controls and depression model mice. Mouse spleen tissues were first cut into small pieces and then digested with collagenase and erythrocyte lysis buffers. After centrifugation, cells were collected and cultured in the RPMI medium.

Mouse primary lung epithelial cells and fibroblast cells were isolated from lung tissues of normal controls and depression model mice. Briefly, mouse lung tissues were first cut into small pieces and then digested with collagenase and erythrocyte lysis buffers. After centrifugation, the cell suspension was inoculated in a culture and let stand for 20 min. Then the cell suspension was transferred into another culture flask. After another 20 min, the above operation to separate epithelial cells and fibroblasts was repeated. These cells were collected separately and cultured in the RPMI medium. Mouse MEFs were prepared from the mouse embryos at day 13.5 and were cultured in DMEM supplemented with 10% FBS. Mouse PBMCs were isolated from freshly collected blood using a Lymphocyte Separation Medium (Da you, DAKEWE).

Cell culture and reagents

RAW264.7 and A549 cells were obtained from ATCC. Cells were cultured at 37 °C under 5% CO_2 in DMEM (HyClone) supplemented with 10% FBS (GIBCO, Life Technologies), 100 units/mL penicillin, and 100 μg/mL streptomycin. Recombinant human IFNα was purchased from the PBL Interferon Source. Recombinant mouse IFNβ was purchased from R&D Systems. Meptazinol, PR-619 and Conivaptan were purchased from Selleck. Arginine vasopressin and Dexamethasone were purchased from Sangon Biotech. Corticotropin was purchased from Yuanye Biotechnology. CHX and other chemicals were purchased from Sigma. Morphine was obtained from the First Affiliated Hospital of Soochow University.

Plasmids and transfection

Myc-AHI1 plasmids were from Dr. Xinshun Xu (Soochow University, China). Flag-OTUD1 plasmids were obtained from Dr. J Wade Harper (Harvard Medical School). Myc-OTUD1 was generated using PCR methods. The Myc-OTUD1-C320A-H431Q mutant (CH) was generated by the QuickChange Lightning site-Directed Mutagenesis Kit (Stratagene, 210518). HA-ubiquitin (HA-Ub), HA-K48, HA-K63 were from Dr. Lingqiang Zhang (State Key Laboratory of Proteomics, Beijing). HA-Tyk2, ISRE-Luc and Renilla plasmids were gifts from Dr. Serge Y. Fuchs (University of Pennsylvania). Flag-ubiquitin (Flag-Ub) was a gift from Dr. Feng Shao (National Institute of Biological Sciences, Beijing). The shOTUD1 plasmid was purchased from GENECHEM (Shanghai, China). The two shAHI1 plasmids were constructed in the shX vector (from Dr. Jianfeng Dai in Soochow University) with following primers:

shAHI1(#1)-forward: 5'-CACCGCGGAGACATTATCCGAGTGTTCGAAAACACTCGGATAATGTCTCCG-3';

shAHI1(#1)-reverse: 5'-AAAACGGAGACATTATCCGAGTGTTTTCGAACACTCGGATAATGTCTCCGC-3';

shAHI1(#2)-forward: 5'-CACCGCCATATTGGTCCGACAGTTTCGAAAAACTGTCGGACCAATATGGC-3';

shAHI1(#2)-reverse: 5'-AAAAGCCATATTGGTCCGACAGTTTTTCGAAACTGTCGGACCAATATGGC-3'.

Transient transfections were carried out using LongTrans (Ucallm, TF/07), LipoMax (Sudgen, 32011) or GenePORTER2 (Genlantis, T202015) according to manufacturer's instructions. For transfection of macrophages, a single-well nucleofection instrument (Lonza VCA-1003) was used. Briefly, 1×10^6 RAW264.7 cells were incubated with 300 ng DNA in 100 μL nucleofector solution, and immediately were put into the nucleofector device. The nucleofector program D-032 was used.

Mass spectrometry (MS) analysis

SDS-PAGE gels were minimally stained with the Silver Staining kit (Beyotime, P0017S). Then the gels were cut into 1 × 1 mm gel block and digested with trypsin. The resulting tryptic peptides were purified using a C18 Zip Tip. Next, the peptides were analyzed by an Orbitrap Elite hybrid mass spectrometer

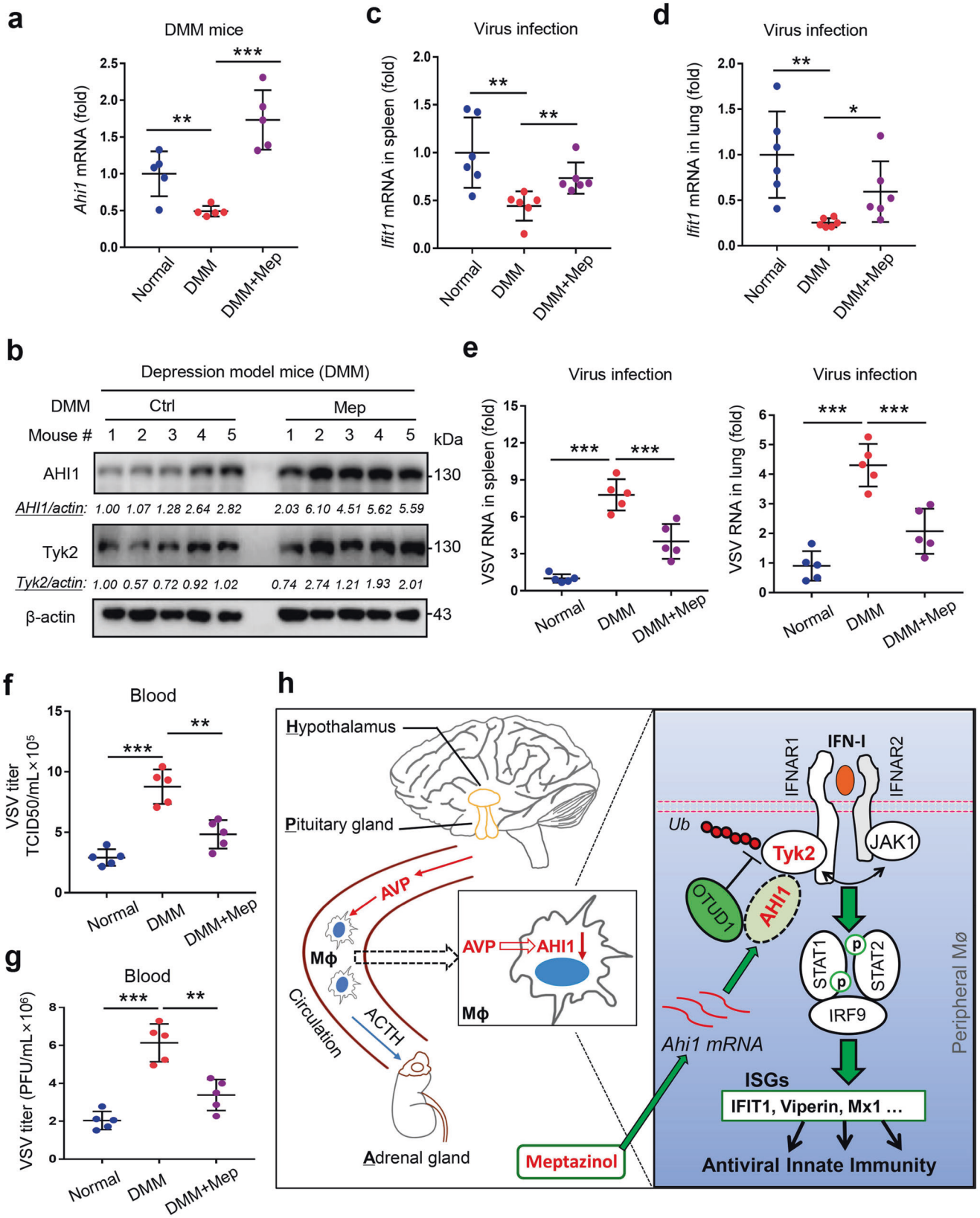

(Thermo Fisher) coupled with the Dionex LC. MS/MS spectra were collected for the selected precursor ion within a 0.02 Da mass isolation window. All spectral data were searched using the Proteome Discoverer 1.4 against a UniProt protein database (https://www.uniprot.org). The peptide spectrum matches for OTUD1 were obtained after database search.

Immunoblotting and immunoprecipitation

Cells were harvested using the NP-40 lysis buffer that contains 150 mM NaCl, 20 mM Tris-HCl (pH 7.4), 0.5 mM EDTA, 1% Nonidet P-40 (NP-40), PMSF (50 μg/mL) and protease inhibitor mixtures (Sigma). After centrifugation at 12,000× *g* for 15 min, protein concentrations were measured and

Fig. 8 Meptazinol improves in vivo AHI1 and Tyk2 levels and enhances antiviral immunity in depression model mice. a Depression model mice were administrated with physiological saline or meptazinol (Mep, 10 mg/kg; i.p.) for 48 h. RT-qPCR was used to analyze *Ahi1* mRNA levels in the spleen tissues of normal control mice (Normal) and depression model mice. **b** Western blot analysis of AHI1 and Tyk2 protein levels in the spleen tissues of depression model mice administrated with physiological saline (Ctrl) or Mep as **a**. **c**, **d** RT-qPCR analysis of the *Ifit1* mRNA levels in the spleen (**c**) and lung (**d**) tissues of mice administrated with Mep as **a** and then infected with VSV (1×10^8 PFU/g of body weight; i.p.) for 24 h. **e** RT-qPCR analysis of VSV RNA levels in the spleen (left) and lung (right) tissues of mice administrated with Mep as **a** and then infected with VSV (1×10^8 PFU/g of body weight; i.p.) for 24 h. **f** $TCID_{50}$ assay of VSV titers in the blood from mice administrated with Mep as **a** and then infected with VSV as **c**. **g** Plaque assay of VSV titers in the blood from mice administrated with Mep as **a** and then infected with VSV as **c**. **h** The proposed model of depression-mediated antiviral immune dysfunction. AVP from the HPA system induces AHI1 reduction in macrophages and peripheral tissues, which disrupts AHI1-mediated stabilization of cellular Tyk2 by the deubiquitinase OTUD1, thus attenuating IFN-I antiviral immune activity. $^*P < 0.05$, $^{**}P < 0.01$ and $^{***}P < 0.001$ (two-tailed unpaired Student's *t*-test). All graphs show the means ± SEM for five individual mice (**a**, **c**–**g**). Data are representative of three independent experiments (**b**).

equal amounts of lysates were used for either immunoblotting or immunoprecipitation. Immunoprecipitation was performed using specific antibodies on a rotor at 4 °C. Protein G agarose beads (Millipore, #16-266) were added into samples and incubated on a rotor at 4 °C. After washed five times with the lysis buffer, the immunoprecipitates were eluted by boiling with the loading buffer containing β-mercaptoethanol for 10 min and analyzed by SDS-PAGE, followed by transferring to PVDF membranes. Membranes were then blocked with 5% non-fat milk for 30 min at room temperature and then probed with the primary antibodies, followed by incubation with the anti-mouse or anti-rabbit (Bioworld) secondary antibodies. Immunoreactive bands were visualized with a SuperSignal West Dura Extended kit (Thermo Scientific). The antibodies with indicated dilutions were as follows: AHI1 (Santa Cruz, sc-515382, 1:500), JAK1 (Santa Cruz, sc-1677, 1:1000), Tyk2 (Cell Signaling Technology, 14193, 1:1000), STAT1 (Cell Signaling Technology, 9172, 1:1000), STAT2 (Cell Signaling Technology, D9J7L, 1:1000), IRF9 (Abcam, ab51639, 1:1000), IFNAR1 (Sino Biological, 13222-H08H, 1:1000), IFNAR2 (Santa Cruz, sc-137209, 1:1000), OTUD1 (Abcam, ab122481, 1:1000), Flag (Sigma, F7425, 1:5000), HA (Abcam, ab9110, 1:3000), Myc (Abmart, M20002H, 1:3000), pY701-STAT1 (Cell Signaling Technology, 9167, 1:1000), VSV-G (Santa Cruz, sc-66180, 1:1000), Tyk2 (Affinity, AF5223, 1:1000), β-Actin (Proteintech, 66009-1-Ig, 1:2000), Tubulin (Proteintech, 66031-1-Ig, 1:3000), Ubiquitin (Ub) (Santa Cruz, sc-8017, 1:500), K48-Ub (Cell Signaling Technology, 8081, 1:1000).

When protein ubiquitination was determined, cells were harvested in the RIPA lysis buffer containing N-ethylmaleimide (10 mM). The immunoprecipitates were washed three times with the high-salt (500 mM NaCl) washing buffer and twice with the normal (150 mM NaCl) washing buffer, and then were subjected to immunoblotting analysis as above.

RNA isolation and real-time quantitative PCR (RT-qPCR)

Total RNAs were isolated from the cells or mouse tissues using a TRIzol reagent (TAKARA). The cDNA was synthesized from 1 μg of total RNA using the RevertAid First Strand cDNA Synthesis kit (Thermo #K1622) and subjected to RT-qPCR with different primers in the presence of SYBR Green Supermix (BIO-RAD) using a StepOne Plus real-time PCR system (Applied Bioscience). A list of all primer sequences was in Supplementary information, Table S1.

The relative expression of the target genes was normalized to *β-actin* or *GAPDH* mRNA. The results were analyzed from three independent experiments and shown as means ± SD.

Flow cytometry and flow sorting

For flow cytometry analysis, cell surface staining was performed using PE-conjugated anti-IFNAR1 (SinoBiological, 50469-R110-P), PE-conjugated anti-IFNAR2 (R&D Systems, ABVR0220021), PerCP-Cy5.5-conjugated anti-mouse Ly6G (BD Bioscience, 560602), FITC-conjugated anti-mouse CD11b (BD Bioscience, 553310), and Alexa Fluor 700-conjugated anti-mouse CD45 (BioLegend, 103128). Cell staining was performed at 4 °C for 30 min and acquired with BD FACS Canto II. FACS data were analyzed using a FlowJo software (FlowJo). For flow sorting, PBMCs were collected with cold 1× PBS and incubated for 30 min at 4 °C with either the FITC anti-human CD3 (eBioscience, 4312299) (T cells), the Alexa-Flour 488 anti-human CD19 (Biolegend, 302219) (B cells), or the PerCP-Cy5.5 anti-human CD14 (BD Bioscience, 550708). After washing, the cells were subjected to sorting using the BD FACS Canto II.

Cycloheximide (CHX) pulse chase assay

The half-life of Tyk2 proteins was examined by a CHX pulse chase assay. Briefly, cells were transfected with control shRNAs, or shAHI1, or shOTUD1. Seventy-two hours after transfection, cells were treated with either DMSO or CHX (50 μg/mL) for 0, 6 and 12 h. Western blotting assay was used to analyze Tyk2 protein levels using an anti-Tyk2 antibody.

ELISA

Depression model mice were made in male ICR mice by a spatial restraint stress model for three weeks. Then the concentrations of mouse AVP in serum were measured using the ELISA kit (Zhenke Biotechnology, Cat# 202107) according to the manufacturer's instructions. For healthy donors and MDD patients, their blood samples were collected and the concentrations of AVP in serum were measured using the ELISA kit (Zhenke Biotechnology, Cat# ZK-1268) according to the manufacturer's instructions.

Reporter gene assay

Cells were transfected with the ISRE-luciferase and Renilla plasmids, together with the specific constructs (shCtrl or shAHI1). Seventy-two hours after transfection, cells were treated with mouse IFNβ (mIFNβ) for 20 h. The luciferase activities were determined by the Dual-luciferase Reporter Assay System (Promega, #E1910) according to the manufacturer's protocol. All activities were assayed from three independent experiments and shown as means ± SD.

Immunofluorescence microscopy

Cells were infected with VSV-GFP (MOI = 0.1) for 24 h. Then cells were subjected to analysis by immunofluorescence microscopy. VSV-GFP viruses were imaged with an upright fluorescence microscope at a 200× magnification.

$TCID_{50}$ assay and Viral plaque assay

Viral titers were determined by a standard 50% tissue culture-infective dose ($TCID_{50}$) assay. Cells transfected with different plasmids were infected with VSV for 24 h. Mice were given intraperitoneal injections (i.p.) of VSV (1×10^8 PFU/g of body weight) for 24 h. Cultured supernatants or serum of mice containing VSV viruses were serially diluted with DMEM and then placed on the monolayer of Vero cells in 96-well plates. The $TCID_{50}$ was calculated using the Spearman-Karber algorithm. For VSV plaque assay, supernatants from mouse peritoneal macrophages or serum from mice infected VSV were harvested and then were diluted $1{:}10^4$ to $1{:}10^8$, and then were used for infection of Vero cells plated on 12-well plates. For HSV plaque assay, supernatants from mouse peritoneal macrophages infected HSV were harvested and then were diluted $1{:}10^1$ to $1{:}10^4$, and were used for infection of Vero cells plated on 12-well plates. For H1N1 plaque assay, supernatants from mouse peritoneal macrophages infected H1N1 were harvested and then were diluted $1{:}10^2$ to $1{:}10^5$, and were used for infection of Vero cells plated on 12-well plates. At 1 h after infection, the supernatants were removed and cells were washed with PBS, and medium containing 0.6% low melting agar and 5% FBS was overload onto the cells. At 2–3 days after infection, cells were fixed for 2–3 h with 4% formaldehyde and were stained with 0.1% crystal violet. Plaques were counted, and results were averaged and multiplied by the dilution factor for calculation of viral titers as PFU/mL.

RNA sequencing analysis

Total RNAs were qualified and quantified using a Nano Drop and Agilent 2100 bioanalyzer (Thermo Fisher Scientific, MA, USA). Oligo(dT)-attached magnetic beads were used to purify mRNA. Purified mRNA was fragmented into small pieces with fragment buffer. Then first-strand cDNA

was generated using random hexamer-primed reverse transcription, followed by a second-strand cDNA synthesis. Afterwards, A-Tailing Mix and RNA Index Adapters were added by incubating to end repair. The cDNA fragments obtained were amplified by PCR, and products were purified by Ampure XP Beads, then dissolved in EB solution. The products were validated on the Agilent Technologies 2100 bioanalyzer for quality control. The double-stranded PCR products were heated denatured and circularized by the splint oligo sequence to get the final library. The single-strand circle DNA (ssCir DNA) was formatted as the final library. The final library was amplified with phi29 to make DNA nanoball (DNB) which had more than 300 copies of one molecular. DNBs were loaded into the patterned nanoarray and single-end 50-base reads were generated on BGIseq500 platform (BGI-Shenzhen, China). Raw data (raw reads) were processed using SOAPnuke (v1.5.2). The reads containing poly-N and low-quality reads were removed to obtain the clean reads. Then, the clean reads were mapped to the reference genome using hisat2. Bowtie2 (v2.2.5) was applied to align the clean reads to the reference coding gene set, then gene expression levels were calculated by RSEM (v1.2.12) Gene ontology enrichment and Kyoto Encyclopedia of Genes and Genomes pathway enrichment analysis of differentially expressed genes were respectively performed using R based on the hypergeometric distribution. The RNA sequencing data have been deposited in the Gene Expression Omnibus with accession no. GSE176217.

Viruses and viral infection in vitro

Vesicular stomatitis virus and Sendai virus were gifts from Dr. Chen Wang (China Pharmaceutical University). Herpes Simplex Virus-1 was from Dr. Chunfu Zheng (Fujian Medical University, China). VSV-GFP was from Dr. Chunsheng Dong (Soochow University, China). The antiviral effects of IFNβ were determined by pretreating cells with IFNβ for 20 h prior to viral infection. Briefly, cells were transfected with Myc-AHI1 constructs or AHI1 shRNAs. Forty-eight hours after transfection, cells were pretreated with mIFNβ (40 IU/mL) for 20 h. After washed twice, cells were challenged by VSV-GFP at an MOI = 0.1 in the serum-free medium for 2 h for virus entry. Then the infection medium was removed by washing twice by 1× PBS. Cells were further fed in the fresh 10% FBS medium for 24 h. Then cells were analyzed by immunofluorescence, RT-qPCR or western blot assay. To assess the antiviral ability of cells against HSV-1, cells were collected and viral RNAs were analyzed to detect viral *Ul46* gene by RT-qPCR.

Viral infection in vivo

For in vivo viral infection studies, 6–8-week-old mice (*Ahi1*$^{+/+}$, *Ahi1*$^{-/-}$, normal controls or depression model mice) were infected with VSV (1×10^8 PFU/g of body weight; i.p.). Twenty-four hours after infection, mouse lung, liver, and spleen tissues were obtained and grinded into small pieces. Then RT-qPCR was used to analyze VSV viral RNAs.

Meptazinol and AVP administration in vivo

For in vivo meptazinol studies, Normal controls and depression model mice were given intraperitoneal injections of meptazinol (10 mg/kg). After 48 h, mice were infected with VSV (1×10^8 PFU/g of body weight; i.p.). Twenty-four hours after virus infection, mouse liver, spleen and lung tissues were harvested and then *Ahi1* and ISGs mRNA levels, as well as viral RNA levels, were analyzed by RT-qPCR. In addition, western blot assay was used to analyze AHI1 and Tyk2 protein levels in the spleen tissues.

For in vivo AVP studies, 6–8-week old C57BL/6 mice were given intraperitoneal injections of AVP (50 ng/kg) once a day. After 48 h, mouse PBMCs were harvested and then *Ahi1* and ISGs mRNA levels were analyzed by RT-qPCR. In addition, western blot assay was used to analyze Tyk2 protein levels in the spleen tissues.

Lung histology

Ahi1$^{+/+}$ and *Ahi1*$^{-/-}$mice were intraperitoneally infected with VSV (1×10^8 PFU/g of body weight) for 24 h. Then the lung tissues of mice were fixed in 4% formaldehyde solution and embedded in paraffin. Paraffin sections were stained with H&E solution and then observed for histological changes by light microscopy.

Statistics

Two-tailed unpaired Student's *t*-test was used for the comparison between different groups. All differences were considered statistically significant when $P < 0.05$. *P* values are indicated by asterisks in the figures as followed: $^*P < 0.05$, $^{**}P < 0.01$ and $^{***}P < 0.001$.

REFERENCES

1. Alvarez Retuerto, A. I. et al. Association of common variants in the Joubert syndrome gene (AHI1) with autism. *Hum. Mol. Genet.* **17**, 3887–3896 (2008).
2. Guze, S. B. & Robins, E. Suicide and primary affective disorders. *Br. J. Psychiatry* **117**, 437–438 (1970).
3. Moussavi, S. et al. Depression, chronic diseases, and decrements in health: results from the World Health Surveys. *Lancet* **370**, 851–858 (2007).
4. Leserman, J. HIV disease progression: depression, stress, and possible mechanisms. *Biol. Psychiatry* **54**, 295–306 (2003).
5. Owora, A. H. Major depression disorder trajectories and HIV disease progression: results from a 6-year outpatient clinic cohort. *Medicine* **97**, e0252 (2018).
6. Yanover, C. et al. What factors increase the risk of complications in SARS-CoV-2-infected patients? A cohort study in a nationwide Israeli Health Organization. *JMIR Public Health Surveill.* **6**, e20872 (2020).
7. Liao, C. H., Chang, C. S., Muo, C. H. & Kao, C. H. High prevalence of herpes zoster in patients with depression. *J. Clin. Psychiatry* **76**, e1099–e1104 (2015).
8. Irwin, M. R. et al. Major depressive disorder and immunity to varicella-zoster virus in the elderly. *Brain Behav. Immun.* **25**, 759–766 (2011).
9. Canli, T. Reconceptualizing major depressive disorder as an infectious disease. *Biol. Mood Anxiety Disord.* **4**, 10 (2014).
10. Jones-Brando, L. et al. Atypical immune response to Epstein-Barr virus in major depressive disorder. *J. Affect. Disord.* **264**, 221–226 (2020).
11. Sun, L., Wu, J., Du, F., Chen, X. & Chen, Z. J. Cyclic GMP-AMP synthase is a cytosolic DNA sensor that activates the type I interferon pathway. *Science* **339**, 786–791 (2013).
12. Rehwinkel, J. & Reis E Sousa, C. RIGorous detection: exposing virus through RNA sensing. *Science* **327**, 284–286 (2010).
13. Kawai, T. & Akira, S. The role of pattern-recognition receptors in innate immunity: update on Toll-like receptors. *Nat. Immunol.* **11**, 373–384 (2010).
14. Borden, E. C. et al. Interferons at age 50: past, current and future impact on biomedicine. *Nat. Rev. Drug Discov.* **6**, 975–990 (2007).
15. Sadler, A. J. & Williams, B. R. Interferon-inducible antiviral effectors. *Nat. Rev. Immunol.* **8**, 559–568 (2008).
16. Guo, T. et al. ADP-ribosyltransferase PARP11 modulates the interferon antiviral response by mono-ADP-ribosylating the ubiquitin E3 ligase β-TrCP. *Nat. Microbiol.* **4**, 1872–1884 (2019).
17. Zuo, Y. et al. Regulation of the linear ubiquitination of STAT1 controls antiviral interferon signaling. *Nat. Commun.* **11**, 1146 (2020).
18. Katlinski, K. V. et al. Inactivation of Interferon Receptor Promotes the Establishment of Immune Privileged Tumor Microenvironment. *Cancer Cell* **31**, 194–207 (2017).
19. Huangfu, W. C. et al. Inflammatory signaling compromises cell responses to interferon alpha. *Oncogene* **31**, 161–172 (2012).
20. Ortiz, A. et al. An Interferon-driven oxysterol-based defense against tumor-derived extracellular vesicles. *Cancer Cell* **35**, 33–45.e36 (2019).
21. Xu, X. et al. Neuronal Abelson helper integration site-1 (Ahi1) deficiency in mice alters TrkB signaling with a depressive phenotype. *Proc. Natl. Acad. Sci. USA* **107**, 19126–19131 (2010).
22. Porcelli, S. et al. Abelson helper integration site-1 gene variants on major depressive disorder and bipolar disorder. *Psychiatry Investig.* **11**, 481–486 (2014).
23. Guo, D. et al. Tyrosine hydroxylase down-regulation after loss of Abelson helper integration site 1 (AHI1) promotes depression via the circadian clock pathway in mice. *J. Biol. Chem.* **293**, 5090–5101 (2018).
24. Zhang, L. et al. Induction of OTUD1 by RNA viruses potently inhibits innate immune responses by promoting degradation of the MAVS/TRAF3/TRAF6 signalosome. *PLoS Pathog.* **14**, e1007067 (2018).
25. Wang, B. et al. Ahi1 regulates the nuclear translocation of glucocorticoid receptor to modulate stress response. *Transl. Psychiatry* **11**, 188 (2021).
26. Stark, G. R. & Darnell, J. E. Jr The JAK-STAT pathway at twenty. *Immunity* **36**, 503–514 (2012).
27. Wilks, A. F. The JAK kinases: not just another kinase drug discovery target. *Semin. Cell Dev. Biol.* **19**, 319–328 (2008).
28. Wilks, A. F. & Oates, A. C. The JAK/STAT pathway. *Cancer Surv.* **27**, 139–163 (1996).
29. Luo, Q. et al. OTUD1 Activates Caspase-Independent and Caspase-Dependent Apoptosis by Promoting AIF Nuclear Translocation and MCL1 Degradation. *Adv. Sci.* **8**, 2002874 (2021).
30. Yao, F. et al. SKP2- and OTUD1-regulated non-proteolytic ubiquitination of YAP promotes YAP nuclear localization and activity. *Nat. Commun.* **9**, 2269 (2018).

31. Lu, D. et al. Mutations of deubiquitinase OTUD1 are associated with autoimmune disorders. *J. Autoimmun.* **94**, 156–165 (2018).
32. van Londen, L. et al. Plasma levels of arginine vasopressin elevated in patients with major depression. *Neuropsychopharmacology* **17**, 284–292 (1997).
33. Capuron, L. et al. Association of exaggerated HPA axis response to the initial injection of interferon-alpha with development of depression during interferon-alpha therapy. *Am. J. Psychiatry* **160**, 1342–1345 (2003).
34. Pace, T. W., Hu, F. & Miller, A. H. Cytokine-effects on glucocorticoid receptor function: relevance to glucocorticoid resistance and the pathophysiology and treatment of major depression. *Brain Behav. Immun.* **21**, 9–19 (2007).
35. Musselman, D. L. et al. Higher than normal plasma interleukin-6 concentrations in cancer patients with depression: preliminary findings. *Am. J. Psychiatry* **158**, 1252–1257 (2001).
36. Capuron, L., Ravaud, A., Miller, A. H. & Dantzer, R. Baseline mood and psychosocial characteristics of patients developing depressive symptoms during interleukin-2 and/or interferon-alpha cancer therapy. *Brain Behav. Immun.* **18**, 205–213 (2004).
37. Suzuki, H. et al. Altered populations of natural killer cells, cytotoxic T lymphocytes, and regulatory T cells in major depressive disorder: Association with sleep disturbance. *Brain Behav. Immun.* **66**, 193–200 (2017).
38. Jahangard, L. & Behzad, M. Diminished functional properties of T regulatory cells in major depressive disorder: The influence of selective serotonin reuptake inhibitor. *J. Neuroimmunol.* **344**, 577250 (2020).
39. Alvarez-Mon, M. A. et al. Abnormal distribution and function of circulating monocytes and enhanced bacterial translocation in major depressive disorder. *Front. Psychiatry* **10**, 812 (2019).
40. Patas, K. et al. T cell phenotype and T cell receptor repertoire in patients with major depressive disorder. *Front. Immunol.* **9**, 291 (2018).
41. Schleifer, S. J., Keller, S. E., Bond, R. N., Cohen, J. & Stein, M. Major depressive disorder and immunity. Role of age, sex, severity, and hospitalization. *Arch. Gen. Psychiatry* **46**, 81–87 (1989).
42. Rivero, O. et al. Impact of the AHI1 gene on the vulnerability to schizophrenia: a case-control association study. *PLoS ONE* **5**, e12254 (2010).
43. Ren, L. et al. Loss of Ahi1 impairs neurotransmitter release and causes depressive behaviors in mice. *PLoS ONE* **9**, e93640 (2014).
44. Weng, L. et al. Loss of Ahi1 affects early development by impairing BM88/Cend1-mediated neuronal differentiation. *J. Neurosci.* **33**, 8172–8184 (2013).
45. Flammer, J. R. et al. The type I interferon signaling pathway is a target for glucocorticoid inhibition. *Mol. Cell. Biol.* **30**, 4564–4574 (2010).
46. Jin, W. Regulation of BDNF-TrkB signaling and potential therapeutic strategies for Parkinson's Disease. *J. Clin. Med.* **9**, 257 (2020).

ACKNOWLEDGEMENTS

We thank Dr. S.Y. Fuchs (University of Pennsylvania), Dr. J.W. Harper (Harvard Medical School), Dr. F. Shao (National Institute of Biological Sciences, Beijing), Dr. C. Wang (China Pharmaceutical University), Dr. G.Q. Chen (Shanghai Jiaotong University), Dr. L. Zhang (State Key Laboratory of Proteomics, Beijing), Dr. C. Dong and J. Dai (Soochow University) and C. Zheng (Fujian Medical University) for important reagents. We also thank Chenxi Irene Zheng in the Suzhou Industrial Park Xinghai Experimental Middle School for making the proposed model. This work was supported by grants from the National Key R&D Program of China (2017YFE0103700, 2018YFC1705500 and 2018YFC1705505), the National Natural Science Foundation of China (31770177, 31970846, 81120108011, 81771454, and 82071511), Jiangsu Provincial Distinguished Young Scholars (BK20130004), the Priority Academic Program Development of Jiangsu Higher Education Institutions (PAPD).

AUTHOR CONTRIBUTIONS

H.-G.Z., B.W., Junjie W., N.X., Y.M., Q.W., T.G., Y.Yuan, Y.Z., X.C. and T.R. performed the experiments. B.W., Y.Yang, X.L., S.L., Jun W., M.S. and X.X. assisted with collection and analysis of healthy controls and MDD patients. B.W., Junjie W. and N.X. helped with the depression mouse model. H.R. assisted with the RNA-Seq analysis. H.Z., X.X. and H.-G.Z. designed experiments, analyzed data and wrote the manuscript. H.Z., X.X., C.D., Jun W., and M.S. discussed the manuscript. H.Z. and X.X. was responsible for research supervision, coordination, and strategy.

COMPETING INTERESTS

The authors declare no competing interests.

ADDITIONAL INFORMATION

Supplementary information The online version contains supplementary material available at https://doi.org/10.1038/s41422-022-00689-9.

Correspondence and requests for materials should be addressed to Xingshun Xu or Hui Zheng.